

Fault Tolerant Sliding Mode Control Design with Piloted Simulator Evaluation

H. Alwi, C. Edwards, O. Stroosma and J. A. Mulder

Abstract

This paper considers sliding mode allocation schemes for fault tolerant control. The schemes allow redistribution of the control signals to the remaining functioning actuators when a fault or failure occurs. The paper analyzes the schemes and determines conditions under which closed-loop stability is retained for a certain class of faults and failures. It is shown that faults and even certain total actuator failures can be handled directly without reconfiguring the controller. The results obtained from implementing the controllers on the SIMONA research flight simulator, configured to represent a B747 aircraft, show good performance in both nominal and failure scenarios even in wind and gust conditions.

NOMENCLATURE

6-DOF	= 6 degree of freedom
EPR	= engine pressure ratio
cmd	= command signal
ru, rl	= upper and lower rudders
sp	= spoiler
air, ail, aor, aol	= inner right, inner left, outer right and outer left ailerons
p, q, r	= roll, pitch and yaw rate (rad/sec)
V_{tas}	= true air speed (m/s)
α, β	= angle of attack and sideslip angle (rad)
ϕ, θ, ψ	= roll, pitch and yaw angle (rad)
h_e, x_e, y_e	= geometric earth position along the z (altitude), x and y axis (m)
$\bar{\lambda}(\cdot), \underline{\lambda}(\cdot)$	= largest and smallest eigenvalues
$\ \cdot \ $	= Euclidean norm (vectors) or induced spectral norm (matrices)
$u(t)$	= control input
$\nu(t)$	= virtual control input
\mathbb{R}, \mathbb{R}_+	= field of real numbers and the set of strictly positive real numbers
s	= Laplace variable
<i>Subscript</i>	
$lat, long$	= lateral and longitudinal axis

I. INTRODUCTION

Modern aircraft are designed to incorporate actuator redundancy of different forms in order to provide tolerance to faults. Incidents such as the Kalita Air freighter in Detroit, Michigan, October 2004 (which shed an engine mid-flight but was landed safely by the crew) and the DHL flight, Baghdad, November 2003 (which was hit by a missile on its left wing and lost all hydraulics, but landed safely using only the engines) represent examples of successful landings using clever manipulation of the remaining functional control surfaces after faults/failures have occurred in-flight. The inclusion of actuator redundancy typically results in so-called over actuated systems. Control allocation (CA) has emerged as one potential technique for systematically dealing with over actuated plants. Researchers, for examples Buffington *et al.*[1] and Davidson *et al.*[2] have shown the capabilities of CA for systems with faults and failures. One of the benefits of CA is that the controller structure does not have to be reconfigured in the case of

H. Alwi and C. Edwards are with the College of Engineering, Mathematics and Physical Sciences, University of Exeter, EX4 4QF, UK. h.alwi@exeter.ac.uk, C.Edwards@exeter.ac.uk

O. Stroosma and J. A. Mulder are with the Control and Simulation section of the Faculty of Aerospace Engineering, Delft University of Technology, Kluyverweg 1, 2629HS, The Netherlands. O.Stroosma@tudelft.nl, J.A.Mulder@tudelft.nl

faults and it can deal directly with total actuator failures without requiring reconfiguration/accommodation of the controller, because the CA scheme ‘automatically’ redistributes the control signal.

The insensitivity and robustness properties of sliding mode control to certain types of disturbances and uncertainty (see §3.4 in Edwards & Spurgeon[3]), especially to actuator faults, make it attractive for fault tolerant control (FTC) especially in the area of flight control. Sliding mode controllers (as well as many other traditional control methods) cannot deal directly with actuator failures. However control allocation provides one solution to this problem by providing access to the ‘redundant’ actuators. Therefore, a combination of sliding mode and control allocation provides a powerful tool for the development of simple, robust fault tolerant flight controllers that work for a wide range of faults and failures without requiring any reconfiguration (provided there is enough redundancy in the system).

The work in Shtessel *et al.*[4] and Wells & Hess [5] provides practical examples of the combination of sliding mode control (SMC) and CA for FTC. The work by Shin *et al.*[6] uses control allocation ideas, but formulates the problem from an adaptive controller point of view. However none of these papers provide a detailed stability analysis and discuss sliding mode controller design issues when using control allocation. Recent work by Corradini *et al.*[7] shows that total failures can be dealt with by SMC schemes provided that there is enough redundancy in the system. However, Corradini *et al.*[7] considers exact duplication of actuators to achieve redundancy, whereas in many over actuated real engineering systems, the redundant actuators do not have identical dynamics to the ‘primary’ ones. More recently in Alwi & Edwards [8] a sliding mode control allocation scheme was proposed for a more general class of uncertain linear systems. A set of easily testable conditions was developed to guarantee the stability of the closed-loop system subject to a class of actuator faults. The scheme in Alwi & Edwards [8] uses a control law which depends on (an estimate of) the ‘efficiency/effectiveness’ of the actuators. In this paper, these ideas are extended and an adaptive scheme is proposed which does not depend explicitly on the estimate of actuators ‘efficiency’.

In this paper, the potential of SMC and CA is demonstrated through an implementation of these ideas on an aircraft research motion simulator. The sliding mode control allocation schemes have been designed and tested on an advanced 6 degree of freedom (6-DOF) research flight simulator called SIMONA (SIMulation, MOTion and NAVigation) running a high fidelity non-linear aircraft model based on FTLAB747[9]. The control strategy considered in this paper uses the SMC robustness properties and CAs capability to redistribute the control effort to the remaining functional actuators when faults/failures occur.

II. TEST FACILITIES (SIMONA)

For the study of faults and failures, a high fidelity nonlinear aircraft model can accurately simulate real life conditions and the performance of an aircraft in a safe way. The FTLAB747 software running under MATLAB¹ has been developed for the study of fault tolerant control and fault detection & isolation (FDI) schemes [10]. It represents a ‘real world’ model of a B747-100/200 aircraft with 77 states incorporating rigid body variables, sensors, actuators and aeroengine dynamics. All the control surfaces and engine dynamics are modelled with realistic position limits and rate limits. The software was originally developed at Delft University of Technology by van der Linden (Delft University Aircraft Simulation and Analysis Tool, DASMAT) [11] and Smaili (Flight Lab 747, FTLAB747) [12], and later developed and enhanced for use in terms of fault detection and fault tolerant control by Marcos & Balas [10] (FTLAB747 V6.1/V6.5). This software has been used as a realistic platform to test FTC and FDI schemes by many researchers (see for example Marcos *et al.*[13], Szaszi *et al.*[14], Maciejowski & Jones [15]). More recently this software has been upgraded to V6.5/7.1/2006b by Smaili *et al.*[9] to allow all the control surfaces to be controlled independently offering more degrees of control flexibility especially during faults or failures.

The SIMONA (SIMulation, MOTion and NAVigation) Research Simulator (SRS) in Figure 1 is a pilot-in-the-loop flight simulator operated by the Delft University of Technology. It provides researchers with a powerful tool that can be adapted to various uses [16]: for example research into human (motion) perception [17], [18], [19], aircraft handling qualities [20], [21], fly-by-wire control algorithms and flight deck displays [22], [23], flight procedures [24], [25] and air traffic control [26]. The simulator’s flexible software architecture and high-fidelity cueing environment allows the integration of the B747 model from Smaili *et al.* [9]. Its inputs and outputs were standardized to fit the SRS software environment and the SIMULINK model was converted to C code using Real-Time Workshop. Finally

¹MATWORKS trademark

the model was integrated with the pilot controls, aircraft instruments (Figure 1(b)) and other cueing devices of the SRS (i.e. outside visual and motion systems). On the flight deck of the SRS the evaluation pilot was presented with flight instruments representative of the B747 aircraft, a control column with B747 feel system dynamics, a central pedestal with dual engine controls, a Mode Control Panel (MCP) for controlling the autopilot and a wide collimated view on a virtual outside world. The simulator's motion system was tuned to give the pilot realistic inertial motion cues in nominal and failure conditions.

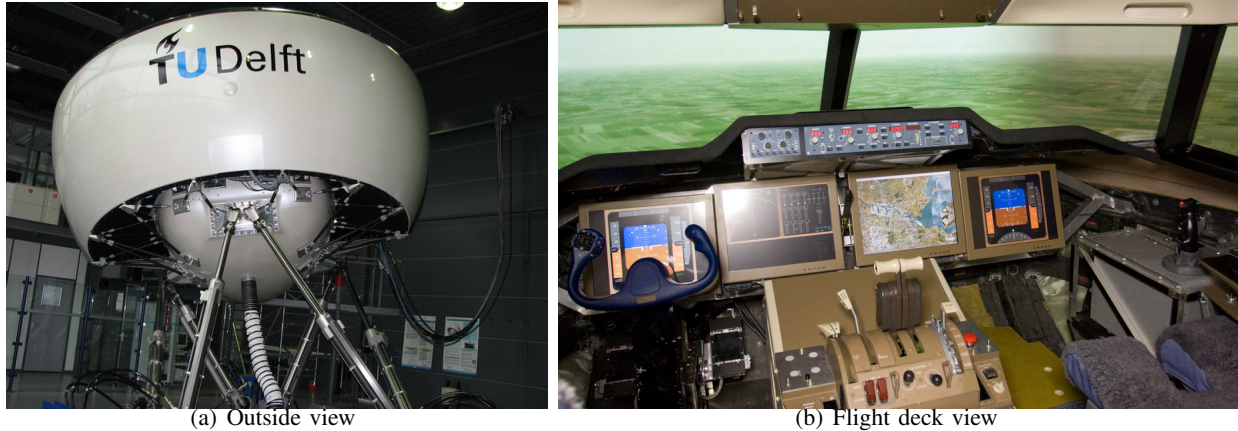


Fig. 1. SIMONA research simulator

III. A SLIDING MODE CONTROL ALLOCATION SCHEME

In this paper, a sliding mode control scheme using control allocation will be designed based on a linearization of the aircraft about an operating condition. This section describes the problem formulation and introduces the control scheme that will be tested.

A. Problem Formulation

This paper considers a situation where a fault associated with the actuators develops in a system. It will be assumed that the system subject to actuator faults or failures, can be written as

$$\dot{x}(t) = Ax(t) + Bu(t) - BK(t)u(t) + BK(t)d(t) \quad (1)$$

where $A \in \mathbb{R}^{n \times n}$ and $B \in \mathbb{R}^{n \times m}$. The effectiveness gain $K(t) = \text{diag}(k_1(t), \dots, k_m(t))$ where the $k_i(t)$ are scalars satisfying $0 \leq k_i(t) \leq 1$. These scalars model a decrease in effectiveness of a particular actuator. If $k_i(t) = 0$, the i th actuator is working perfectly whereas if $k_i(t) > 0$, a fault is present, and if $k_i(t) = 1$ the actuator has failed completely. The exogenous signal $d(t)$ represents a disturbance which may impact on the system as a result of a fault/failure. For example, the moment generated by a control surface which has stuck in a non-neutral position in control channel i could be modeled as $k_i = 1$ and $d_i \neq 0$.

In most CA strategies, the control signal is distributed equally among all the actuators [6], [4], [5] or distributed based on the limits (position and rate) of the actuators [2], [27], [28]. In this section, equal weight redistribution will be considered to redirect the control signals to the remaining actuators when faults/failures occur. For most systems with actuator redundancy, the assumption that $\text{rank}(B) = l < m$, often employed in the literature, is not valid. However, often the system states can be reordered, and the matrix B from (1) can be partitioned as:

$$B = \begin{bmatrix} B_1 \\ B_2 \end{bmatrix} \quad (2)$$

where $B_1 \in \mathbb{R}^{(n-l) \times m}$ and $B_2 \in \mathbb{R}^{l \times m}$ has rank l . The partition is in keeping with the notion of splitting the control law from the control allocation task [28], [2]. In aircraft systems, B_2 is associated with the equations of angular acceleration in roll, pitch and yaw [28]. Here it is assumed that the matrix B_2 represents the dominant contribution of the control action on the system, while B_1 generally will have elements of 'small' magnitude compared with

$\|B_2\|$. Compared to the work in Shin *et al.*[6] where it is assumed that $B_1 = 0$, here $B_1 \neq 0$ will be considered explicitly in the controller design and in the stability analysis. It will be assumed without loss of generality that the states of the system in (1) have been transformed so that $B_2 B_2^T = I_l$ and therefore $\|B_2\| = 1$. This is always possible since $\text{rank}(B_2) = l$ by construction. As in Alwi & Edwards [8], let the ‘virtual control’ $\nu(t)$ be defined as

$$\nu(t) := B_2 u(t) \quad (3)$$

so that

$$u(t) = B_2^\dagger \nu(t) \quad (4)$$

where the pseudo inverse is chosen as

$$B_2^\dagger := \Omega B_2^T (B_2 \Omega B_2^T)^{-1} \quad (5)$$

and $\Omega \in \mathbb{R}^{m \times m}$ is a symmetric positive definite (s.p.d) diagonal weighting matrix. It can be shown that the pseudo-inverse in (5) arises from the optimization problem

$$\min_{u(t)} u(t)^T \Omega^{-1} u(t) \quad \text{subject to } B_2 u(t) = \nu(t) \quad (6)$$

In Alwi & Edwards [8], the weighting matrix was chosen to be $\Omega(t) = I - K(t)$. The effect of this choice is that $u(t)$ in (4) depends explicitly on $K(t)$ because B_2^\dagger from (5) does. Here instead, and perhaps more conventionally,

$$\Omega := I \quad (7)$$

With this choice of weighting matrix, equation (4) becomes

$$u(t) = B_2^\dagger \nu(t) = B_2^T \underbrace{(B_2 B_2^T)^{-1}}_I \nu(t) = B_2^T \nu(t) \quad (8)$$

In Alwi & Edwards [8], sliding mode control (SMC) techniques[3], have been used to synthesize the ‘virtual control’ $\nu(t)$. Define a switching function $s(t) : \mathbb{R}^n \rightarrow \mathbb{R}^l$ to be

$$s(t) = Sx(t)$$

and let \mathcal{S} be the hyperplane defined by $\mathcal{S} = \{x(t) \in \mathbb{R}^n : Sx(t) = 0\}$. If a control law can be developed which forces the closed-loop trajectories onto the surface \mathcal{S} in finite time and constrains the states to remain there, then an ideal sliding motion is said to have been attained (see §3.2 in Edwards & Spurgeon[3]).

In terms of the stability analysis which follows, the effect of the exogenous disturbance $d(t)$ from (1) is ignored. Clearly this external signal does not affect the stability or otherwise of the closed-loop system – although of course it affects the closed-loop performance of the system. In the following stability analysis $d \equiv 0$. Using a change of coordinates $x \mapsto T_r x(t) = \hat{x}(t)$ where

$$T_r := \begin{bmatrix} I & -B_1 B_2^T \\ 0 & I \end{bmatrix} \quad (9)$$

it is shown in Alwi & Edwards [8] that (1) becomes (in the new coordinate system)

$$\dot{\hat{x}}(t) = \hat{A} \hat{x}(t) + \underbrace{\begin{bmatrix} 0 \\ I \end{bmatrix}}_{\hat{B}_\nu} \nu(t) - \begin{bmatrix} -B_1 B_2^N (I - K) B_2^T \\ I - B_2 (I - K) B_2^T \end{bmatrix} \nu(t) \quad (10)$$

where $\hat{A} := T_r A T_r^{-1}$ and

$$B_2^N := (I - B_2^T B_2) \quad (11)$$

The last term in (10) is zero in the fault free case ($K = 0$), but is treated as (unmatched) uncertainty when $K \neq 0$. Define

$$W = I - K \quad (12)$$

and write

$$B_2^+ := W B_2^T (B_2 W B_2^T)^{-1} \quad (13)$$

It is shown in Alwi & Edwards [8] that there is an upper bound on the norm of the pseudo-inverse B_2^+ in (13) which is independent of W , so that there exists a γ_0 such that

$$\|B_2^+\| = \|WB_2^T(B_2WB_2^T)^{-1}\| < \gamma_0 \quad (14)$$

for all $W = \text{diag}(w_1 \dots w_m)$ such that $0 < w_i \leq 1$. For the system in the $\hat{x}(t)$ coordinates in (10), a suitable choice for the sliding surface is

$$\hat{S} = ST_r^{-1} = \begin{bmatrix} M & I_l \end{bmatrix} \quad (15)$$

where $M \in \mathbb{R}^{l \times (n-l)}$ represents design freedom. Introduce another transformation so that $\hat{x} = (\hat{x}_1, \hat{x}_2) \mapsto T_s x = (\hat{x}_1, s(t))$, where $\hat{x}_1 \in \mathbb{R}^{(n-l)}$ associated with the nonsingular matrix

$$T_s = \begin{bmatrix} I & 0 \\ M & I \end{bmatrix} \quad (16)$$

Equation (10) then becomes

$$\begin{bmatrix} \dot{\hat{x}}_1(t) \\ \dot{s}(t) \end{bmatrix} = \begin{bmatrix} \tilde{A}_{11} & \tilde{A}_{12} \\ \tilde{A}_{21} & \tilde{A}_{22} \end{bmatrix} \begin{bmatrix} \hat{x}_1(t) \\ s(t) \end{bmatrix} + \begin{bmatrix} 0 \\ I \end{bmatrix} \nu(t) - \begin{bmatrix} -B_1B_2^NWB_2^T \\ I - MB_1B_2^NWB_2^T - B_2WB_2^T \end{bmatrix} \nu(t) \quad (17)$$

where $\tilde{A}_{11} := \hat{A}_{11} - \hat{A}_{12}M$, $\tilde{A}_{21} := M\tilde{A}_{11} + \hat{A}_{21} - \hat{A}_{22}M$. If (A, B_ν) is controllable, then $(\hat{A}_{11}, \hat{A}_{12})$ is controllable (see §3.4 in Edwards & Spurgeon[3]) and so M can always be chosen to make $\hat{A}_{11} - \hat{A}_{12}M$ stable. If a control law can be designed to induce sliding, then, the reduced order sliding motion is governed by

$$\dot{\hat{x}}_1(t) = \tilde{A}_{11}\hat{x}_1(t) - B_1B_2^NB_2^+(I + MB_1B_2^NB_2^+)^{-1}\tilde{A}_{21}\hat{x}_1(t) \quad (18)$$

Define

$$\gamma_1 := \|MB_1B_2^N\| \quad (19)$$

then it follows that $\|MB_1B_2^NB_2^+\| < \|MB_1B_2^N\|\|B_2^+\| < \gamma_0\gamma_1$. Since B_2^+ is independent of M , the term γ_0 can be calculated a-priori using the boundedness result from equation (14). If the design matrix M can also be chosen so that γ_1 from (19) satisfies $\gamma_0\gamma_1 < 1$, this guarantees $((I + MB_1B_2^NB_2^+)(B_2WB_2^T))^{-1}$ exists for all W and so the last expression in (18) is well defined.

Remark 1: In a fault free condition, $W = I$ and therefore $B_2^+|_{W=I} = B_2^T$ since $B_2B_2^T = I$. Also

$$B_2^NB_2^+ = (I - B_2^TB_2)B_2^+ = (I - B_2^TB_2)B_2^T = 0$$

and the system in (18) ‘collapses’ to $\dot{\hat{x}}_1(t) = \tilde{A}_{11}\hat{x}_1(t)$ which is the nominal sliding mode reduced order system for which M has been designed to guarantee stability. The system in (18) depends on W and so stability needs to be established.

Define

$$\tilde{G}(s) := \tilde{A}_{21}(sI - \tilde{A}_{11})^{-1}B_1B_2^N \quad (20)$$

where s represents the Laplace variable. By construction the transfer function matrix $\tilde{G}(s)$ is stable. If

$$\gamma_2 = \|\tilde{G}(s)\|_\infty \quad (21)$$

then, it is shown in Alwi & Edwards [8] that during a fault or failure condition, for any combination of $0 < w_i \leq 1$, the closed-loop system will be stable if

$$0 < \frac{\gamma_2\gamma_0}{1 - \gamma_1\gamma_0} < 1 \quad (22)$$

where the scalar γ_0 is defined in (14), the positive scalar γ_1 is defined in (19) and γ_2 is defined in (21).

Remark 2: Both γ_1 and γ_2 depend on the design of the sliding surface since they depend on M ; however they are independent of W . The scalar γ_0 depends on W but is independent of M .

Remark 3: If $B_1 = 0$ (which is an assumption in many schemes: for example Shin *et al.*[6]), then $\gamma_1 = 0$ and $\gamma_2 = 0$ and equation (22) is trivially satisfied. Furthermore, as $\|B_1\| \rightarrow 0$, the scalar $\frac{\gamma_2\gamma_0}{1 - \gamma_1\gamma_0} \rightarrow 0$ and so the requirements of equation (22) are satisfied. This means loosely speaking, for weakly coupled systems in which

$\|B_1\|$ is small, the approach will be feasible. The situation where $B_1 = 0$ can be regarded as the special extreme case as $\|B_1\| \rightarrow 0$.

In Alwi & Edwards [8], a unit vector controller using knowledge of $W(t) = I - K(t)$ was developed to induce a sliding motion. This requires a FDI scheme to estimate $W(t)$ in real-time. In the next subsection, to circumvent this, a different control law will be proposed which does not require the $W(t)$. In this regard the FTC scheme which is proposed is ‘passive’[29] and does not rely on an FDI scheme.

1) *Adaptive Nonlinear Gain*: The proposed control law has a structure given by $\nu(t) = \nu_l(t) + \nu_n(t)$ where

$$\nu_l(t) := -\tilde{A}_{21}\hat{x}_1(t) - \tilde{A}_{22}s(t) \quad (23)$$

and $\nu_n(t)$ represents a nonlinear unit vector term. In a fault free situation it is not necessary and indeed is not advisable to have a large gain on the switched term – therefore ideally the nonlinear gain term should only adapt to the onset of a fault and react accordingly. It is easy to see from (23) that

$$\|\nu_l(t)\| < l_1\|x(t)\| + l_2 \quad (24)$$

where l_1 and l_2 are known positive constants. Consider the following expression for the nonlinear control law component

$$\nu_n(t) := -(\rho(t, x) + \eta) \frac{s(t)}{\|s(t)\|} \quad \text{for } s(t) \neq 0 \quad (25)$$

where η is a positive scalar and the gain ρ is defined to be

$$\rho(t, x) = r(t)(l_1\|x(t)\| + l_2) \quad (26)$$

The scalar variable $r(t)$ is an adaptive gain which varies according to

$$\dot{r}(t) = a(l_1\|x(t)\| + l_2)D_\epsilon(\|s(t)\|) - br(t) \quad (27)$$

where $r(0) = 0$ and the a and b are positive design constants. The function $D_\epsilon : \mathbb{R} \mapsto \mathbb{R}$ is the nonlinear function

$$D_\epsilon(\|s\|) = \begin{cases} 0 & \text{if } \|s\| < \epsilon \\ \|s\| & \text{otherwise} \end{cases} \quad (28)$$

where ϵ is a positive scalar. (A similar function to (28) is considered in Xu *et al.*[30]). Here, ϵ is set to be small and defines a boundary layer about the surface \mathcal{S} , inside which an acceptably close approximation to ideal sliding takes place. Provided the states evolve with time inside the boundary layer, no adaptation of the switching gains takes place. If a fault occurs, which starts to make the sliding motion degrade so that the states evolve outside the boundary layer i.e. $\|s(t)\| > \epsilon$, then the dynamic coefficients $r(t)$ increase in magnitude, (according to (27)), to force the states back into the boundary layer around the sliding surface.

Remark 4: This adaptation scheme differs from the one in Wheeler *et al.*[31] and is more akin to the gain scheme from Xu *et al.*[30].

The choice of the design parameters η , a , b and ϵ depends on the closed-loop performance specifications and requires some design iteration. In general, η needs to be chosen as the nominal (no fault) gain for the nonlinear component of the control law (25) to ensure that sliding occurs in the fault free system. The parameter ϵ is chosen to be small to form a boundary layer about \mathcal{S} , but not too small to cause unnecessary increases in $\rho(t)$. Thus ϵ dictates how sensitive the adaptive gain $r(t)$ is to changes in $s(t)$. The gain a dictates the rate at which $r(t)$ increases in reaction to faults: a large value for a indicates a fast increase of $r(t)$. On the other hand b dictates the rate at which $r(t)$ decreases to the nominal gain η when the fault has been rectified. A relationship between ϵ , η , a and b will be determined in the proof of the proposition which follows. The choice of these design parameters will be discussed further in §IV. The following lemma will show that $r(t)$ is bounded and motion inside a boundary layer around \mathcal{S} is obtained.

Let \mathcal{W} be the set of faults such that

$$\mathcal{W} = \{(w_1 \dots w_m) \in \underbrace{[0, 1] \times [0, 1] \dots \times [0, 1]}_{m \text{ times}} \mid \underline{\lambda}(B_2WB_2^T) > w > 0\} \quad (29)$$

where w is a strictly positive scalar. Notice that $(w_1, \dots, w_m) \in \mathcal{W} \Rightarrow \det(B_2 W B_2^T) \neq 0$.

Proposition 1: Consider the potentially faulty system represented by (1) with the control law in (23)-(25); then the adaptive gain $r(t)$ remains bounded and the switching states $s(t)$ enter a boundary layer around \mathcal{S} in finite time for any fault condition $(w_1 \dots w_m) \in \mathcal{W}$.

Proof: See appendix. ■

Remark 5: For an appropriate choice of a , b and ϵ , close approximation to ideal sliding can be maintained even in the presence of faults. If $\epsilon = 0$ and $b = 0$, then ideal sliding can be guaranteed since it follows from (50) that the Lyapunov derivative $\dot{V} \leq -w^2 \|s\| (1 - \gamma_1 \gamma_0) \eta$. This means ideal sliding can be attained and maintained in finite time. However this scheme has disadvantages in practice since $r(t)$ may become unbounded in the presence of noise [31].

B. Sliding Mode Controller Design Issues

Based on the stability analysis above, the sliding mode control design problem can be summarized as follows:

- Pre-design calculations:
 - (a) Make an appropriate re-ordering of the states in (1) so that the input distribution matrix B is partitioned to identify B_1 and B_2 .
 - (b) Scale the states so that $B_2 B_2^T = I$.
 - (c) Change coordinates using the linear transformation $x(t) \mapsto \hat{x}(t) = T_r x(t)$, where T_r is given in (9), to achieve the canonical form in (10) and isolate the matrices \hat{A}_{11} , \hat{A}_{12} , \hat{A}_{21} and \hat{A}_{22} .
 - (d) Compute the smallest possible scalar γ_0 so that $\|W^2 B_2^T (B_2 W^2 B_2^T)^{-1}\| < \gamma_0, \forall 0 < W \leq I$. This value is an a-priori calculation and is independent of the choice of sliding surface and control law.
- Design of matrix M :
 - (a) The design objective is to compute M from (15) so that $\tilde{A}_{11} := \hat{A}_{11} - \hat{A}_{12} M$ is stable. This is always possible if (A, B_ν) is controllable.
- Stability analysis:
 - (a) Compute and check if $\gamma_1 := \|M B_1 B_2^N\| < \frac{1}{\gamma_0}$ is satisfied. Otherwise re-design M .
 - (b) Calculate $\tilde{G}(s) := \tilde{A}_{21} (sI - \tilde{A}_{11})^{-1} B_1 B_2^N$. If $\|\tilde{G}(s)\|_\infty := \gamma_2 < \frac{1}{\gamma_0} - \gamma_1$, the closed-loop is guaranteed to be stable $\forall 0 < W \leq I$, since $\gamma_2 < \frac{1}{\gamma_0} - \gamma_1$ ensures inequality (22) in (22) holds. Otherwise consider re-designing the matrix M .
- Obtain the virtual control law using (23), (25) and the actual control law using (8).

C. General Remarks

Note that the above analysis is based on the equal distribution of the virtual control i.e. $\Omega = I$ in the optimization (6) in both the nominal and faulty case. This is a popular choice in the literature [6], [4], [5]. During the SIMONA trials, an on-line control allocation scheme as proposed in Alwi & Edwards [8] has also been tested. The idea in Alwi & Edwards [8] is that, instead of using a fixed weight $\Omega = I$ in (12), the effectiveness level of the actuators $K(t)$ is used to change the weight Ω (i.e. $\Omega = I - K$) to allow the control allocation scheme to efficiently redistribute the control signals to the remaining functioning actuators when a fault or failure occurs. The information necessary to compute Ω online can be supplied by a fault reconstruction scheme as described in Tan & Edwards [32] for example, or by using measurements of the actual actuator deflection compared to the demand which is available in many systems e.g. passenger aircraft. From Alwi & Edwards [8], it can be seen that even though the strategy for the control allocation is different, the design procedure for the sliding surface and the stability analysis (as discussed in III-B) is similar and is subject to the same constraints. The only difference is the definition of control law and the nonlinear gain required to maintain sliding. Here it is proposed that

$$u(t) = B_2^T \nu(t) \quad (30)$$

where $\nu(t)$ is given in (23), (25), (26)–(28). In Alwi & Edwards [8], it is suggested that $u(t)$ has the form

$$u(t) = W B_2^T (B_2 W^2 B_2^T)^{-1} \nu(t) \quad (31)$$

However, the control law proposed in Alwi & Edwards [8] is exactly the same as the one proposed in this paper when $\Omega = I$; for details see Alwi & Edwards [8].

The choice $u(t) = B_2^T \nu(t)$ is simpler. The benefit of the scheme proposed in Alwi & Edwards [8] is that a smaller nonlinear gain is sufficient to maintain sliding due to the efficient redistribution of the control signals. Faulty actuators will have small control signal demands compared to healthy actuators and in fact the control signal sent to a failed actuator will be shut off completely. The disadvantage of this method is that the effectiveness level of each actuator needs to be available. For some systems, this information can be obtained directly by measuring the input and output signals to the actuator or by using a fault estimator such as Tan & Edwards [32]. However for some systems, the effectiveness level of the actuators is difficult to estimate accurately. This has motivated the use of a fixed control allocation scheme proposed in this paper. A drawback is the size of the nonlinear gain which may need to be large when faults or failures occur, to maintain sliding and ensure that stability still holds. A conservatively large nonlinear gain or an adaptive nonlinear gain scheme (as discussed in section III-A1 above) needs to be employed.

IV. CONTROLLER DESIGN

The 12 rigid body states of the B747 aircraft can be divided into 6 longitudinal axis states and 6 lateral and directional axes states which are all determined from the 6-degree of freedom equations of motion. The states are given by $x = [p \ q \ r \ V_{tas} \ \alpha \ \beta \ \phi \ \theta \ \psi \ h_e \ x_e \ y_e]^T$. For the longitudinal axis, the states are pitch rate q , true airspeed V_{tas} , angle of attack α , pitch angle θ and altitude h_e . Meanwhile for the lateral and directional axes, the states are roll rate p , yaw rate r , sideslip angle β , roll angle ϕ and yaw angle ψ . The control surfaces comprise 4 ailerons (inner and outer on each wing), 12 spoilers (2 inner spoilers and 4 outer spoilers on each wing), 2 rudders (upper and lower), 4 elevators (an inner and outer on each left and right elevator), a horizontal stabilizer and 4 engine thrusts (which are controlled via engine pressure ratios (EPR)).

In this paper both lateral and longitudinal control is considered. One of the controller design objectives considered here is to bring a faulty aircraft to a near landing condition. This can be achieved by a change of direction through a 'banking turn' manoeuvre, followed by a decrease in altitude and speed. This can be achieved by tracking appropriate roll angle (ϕ) and sideslip angle (β) commands using the lateral controller, and tracking flight path angle (FPA) and airspeed (V_{tas}) commands using the longitudinal controller. For lateral control, the settling time when there is no fault/failure should be approximately 20sec for ϕ and 20sec for β . If a fault/failure occurs, the tracking requirement is 25sec for ϕ and β . These specifications are chosen to ensure that there is almost zero side force and therefore passenger comfort is maintained (page 233 of Bryson [33]). For longitudinal control, the settling time when there is no failure should be 20sec for FPA and 45sec for V_{tas} . If a failure occurs, the tracking requirement is 30sec for FPA with no difference in the V_{tas} tracking. These specifications are taken from Ganguli *et al.*[34].

A linearization has been obtained around an operating condition of 263,000 Kg, 92.6 m/s true airspeed, and an altitude of 600m at 25.6% of maximum thrust and at a 20deg flap position. The result is a 12th order linear model (separated into two 6th order models) associated with the lateral and longitudinal states. For design purposes, only the first four longitudinal ($x_{long} = [q \ V_{tas} \ \alpha \ \theta]^T$) and lateral states ($x_{lat} = [p \ r \ \beta \ \phi]^T$) have been retained. For lateral control, the 4 individual engine pressure ratios (EPR) and the 4 individual ailerons have been used. The 10 spoilers² have been aggregated to produce two control inputs on each wing (spoilers 1-4, 5, 8 and 9-12 have been grouped respectively). The other input represents rudder deflection (the upper and lower rudder has been aggregated to produce a single control signal). For longitudinal control, the 4 elevators have been aggregated to produce one control input while the 4 longitudinal EPRs can be controlled independently. The other input represents horizontal stabilizer deflection. The following state-space system pairs represent the lateral and longitudinal systems about the trim condition

²Spoilers 6 & 7 are ground spoilers and are not used during flight.

$$A_{lat} = \begin{bmatrix} -1.0579 & 0.1718 & -1.6478 & 0.0004 \\ -0.1186 & -0.2066 & 0.2767 & -0.0019 \\ 0.1014 & -0.9887 & -0.0999 & 0.1055 \\ 1.0000 & 0.0893 & 0 & 0 \end{bmatrix} \quad (32)$$

$$B_{lat} = \begin{bmatrix} -0.0832 & 0.0832 & -0.2285 & 0.2285 & -0.2625 & -0.0678 & 0.0678 \\ -0.0154 & 0.0154 & -0.0123 & 0.0123 & -0.0180 & -0.0052 & 0.0052 \\ 0 & 0 & 0 & 0 & 0.0017 & 0.0006 & -0.0006 \\ 0 & 0 & 0 & 0 & 0 & 0 & 0 \\ 0.2625 & 0.1187 & 0.0246 & 0.0140 & -0.0140 & -0.0246 & \\ 0.0180 & -0.2478 & 0.1269 & 0.0724 & -0.0724 & -0.1269 & \\ -0.0017 & 0.0174 & 0.0005 & 0.0005 & -0.0005 & -0.0005 & \\ 0 & 0 & 0 & 0 & 0 & 0 & 0 \end{bmatrix} \left. \begin{array}{l} \\ \\ \\ \\ \\ \\ \\ \end{array} \right\} \begin{array}{l} B_{lat,2} \\ B_{lat,1} \end{array} \quad (33)$$

and

$$A_{long} = \begin{bmatrix} -0.5137 & 0.0004 & -0.5831 & 0 \\ 0 & -0.0166 & 1.7171 & -9.8046 \\ 1.0064 & -0.0021 & -0.6284 & 0 \\ 1.0000 & 0 & 0 & 0 \end{bmatrix} \quad (34)$$

$$B_{long} = \begin{bmatrix} -0.6228 & -1.3578 & 0.0082 & 0.0218 & 0.0218 & 0.0082 \\ 0 & -0.1756 & 1.4268 & 1.4268 & 1.4268 & 1.4268 \\ -0.0352 & -0.0819 & -0.0021 & -0.0021 & -0.0021 & -0.0021 \\ 0 & 0 & 0 & 0 & 0 & 0 \end{bmatrix} \left. \begin{array}{l} \\ \\ \\ \end{array} \right\} \begin{array}{l} B_{long,2} \\ B_{long,1} \end{array} \quad (35)$$

where the states represent $x_{lat} = [p \ r \ \beta \ \phi]^T$ and $x_{long} = [q \ V_{tas} \ \alpha \ \theta]^T$. The lateral control surfaces are $\delta_{lat} = [\delta_{air} \ \delta_{ail} \ \delta_{aor} \ \delta_{aol} \ \delta_{sp1-4} \ \delta_{sp5} \ \delta_{sp8} \ \delta_{sp9-12} \ \delta_r \ e_{1lat} \ e_{2lat} \ e_{3lat} \ e_{4lat}]^T$ which represent aileron deflection (right & left - inner & outer)(rad), spoiler deflections (left: 1-4 & 5 & right: 8 & 9-12) (rad), rudder deflection (rad) and lateral engine pressure ratios (EPR). The longitudinal control surfaces are $\delta_{long} = [\delta_e \ \delta_s \ e_{1long} \ e_{2long} \ e_{3long} \ e_{4long}]^T$ which represent elevator deflection (rad), horizontal stabilizer deflection (rad), and longitudinal EPR. The partition of B in (33) and (35) shows the terms B_1 and B_2 (although a further change of coordinates is necessary to obtain the form in (2) to scale B_2 to ensure $B_2 B_2^T = I$). The controlled output distribution matrices are

$$C_{c_{lat}} = \begin{bmatrix} 0 & 0 & 1 & 0 \\ 0 & 0 & 0 & 1 \end{bmatrix}, \quad C_{c_{long}} = \begin{bmatrix} 0 & 0 & -1 & 1 \\ 0 & 1 & 0 & 0 \end{bmatrix}$$

which represent the states ϕ and β for lateral control and flight path angle (FPA) and V_{tas} for longitudinal control. These linear models will be used to design the control schemes described in the next sections.

To include a tracking facility, integral action has been included for both longitudinal and lateral control. For the generic system in (1), let $x_r(t)$ represent integral action states:

$$\dot{x}_r(t) = r(t) - C_c x(t) \quad (36)$$

where $C_c \in \mathbb{R}^{l \times n}$ is the distribution matrix associated with the controlled outputs and the differentiable (filtered reference) signal $r(t)$ satisfies

$$\dot{r}(t) = \Gamma (r(t) - r_c) \quad (37)$$

with $\Gamma \in \mathbb{R}^{l \times l}$ a stable design matrix and r_c a constant demand vector (for details see §4.4.2 in Edwards & Spurgeon[3]). Augmenting the states from (32)-(35) with the integral action states and defining $x_a(t) = \text{col}(x_r(t), x(t))$ it follows that

$$\dot{x}_a(t) = A_a x_a(t) + B_a u(t) + B_r r(t) \quad (38)$$

where

$$A_a = \begin{bmatrix} 0 & -C_c \\ 0 & A \end{bmatrix} \quad B_a = \begin{bmatrix} 0 \\ B \end{bmatrix} \quad B_r = \begin{bmatrix} I_p \\ 0 \end{bmatrix} \quad (39)$$

If (A, B) is controllable and (A, B, C_c) does not have any zeros at the origin then (A_a, B_a) is controllable (see §4.4.2 in Edwards & Spurgeon[3]). Define a switching function $s_a(t) : \mathbb{R}^{(n+l)} \rightarrow \mathbb{R}^l$ to be

$$s_a(t) = S_a x_a(t) \quad (40)$$

where $S_a \in \mathbb{R}^{l \times (n+l)}$ and $S_a B_a = I_l$. As in equation (23)-(25), the proposed ‘virtual control’ law comprises two components $\nu(t) = \nu_l(t) + \nu_n(t)$. Now because of the reference signal $r(t)$, the linear component has a feed-forward reference term and so $\nu_l(t) = Lx_a(t) + L_r r(t)$ where $L = -\hat{S}_a \hat{A}_a$ and $L_r = -\hat{S}_a \hat{B}_r$. Here \hat{A} , \hat{B}_r and \hat{S} are the matrices from (39) and (40) after a transformation to achieve the regular form in equation (10) has been performed. The nonlinear component is defined as

$$\nu_n(t) = -\rho(t, x_a) \frac{s_a(t)}{\|s_a(t)\|} \quad \text{for } s_a(t) \neq 0 \quad (41)$$

From (8) it follows that

$$u(t) = B_2^T \nu(t) \quad (42)$$

for an equally distributed control is distributed to all the control surfaces. (For on-line CA control law definition, see Alwi & Edwards [8]).

A. Lateral Controller Design

In normal operation, the ailerons will be the primary control surface for ϕ tracking, whilst the spoilers introduce redundancy. Meanwhile for β tracking, the rudder will be the primary control surface and differential engine thrust is the associated redundancy. It will be assumed that at least one of the control surfaces for both ϕ and β tracking will be available when a fault or failure occurs (i.e. one of either the four ailerons or the four spoilers will be available and one of either the rudder or the four engine thrusts are available). Based on these assumptions, it can be verified from a numerical search that $\gamma_{0_{lat}}$ from (14) is $\gamma_{0_{lat}} = 8.1314$.

The matrix which defines the hyperplane must now be synthesized so that the conditions of (22) are satisfied. A quadratic optimal design has been used to obtain the sliding surface $S_{a_{lat}}$ which depends on the matrix M_{lat} in equation (15) (see for example chapter 9 in Utkin [35] and §4.2.2 in Edwards & Spurgeon[3]) where the symmetric positive definite state weighting matrix has been chosen as $Q_{lat} = \text{diag}(0.005, 0.1, 6, 6, 1, 1)$. The first two terms of Q_{lat} are associated with the integral action and are less heavily weighted. The third and fourth term of Q_{lat} are associated with the equations of the angular acceleration in roll and yaw (i.e. $B_{lat,2}$ term partition in (2)) and thus weight the virtual control term. Thus by analogy to a more typical LQR framework, they effect the speed of response of the closed-loop system. Here, the third and fourth terms of Q_{lat} have been heavily weighted compared to the last two terms to reflect a reasonably fast closed-loop system response. The poles associated with the reduced order sliding motion are $\{-0.0707, -0.3867, -0.3405 \pm 0.1484i\}$. Based on this value of M_{lat} , simple calculations from (19) show that $\gamma_{1_{lat}} = 0.0145$, therefore $\gamma_{0_{lat}} \gamma_{1_{lat}} = 0.1180 < 1$ and so the requirements of (22) are satisfied. Also for this particular choice of sliding surface, $\|G_{lat}(s)\|_\infty = \gamma_{2_{lat}} = 0.0764$ from (21). Therefore from (22),

$$\frac{\gamma_{2_{lat}} \gamma_{0_{lat}}}{1 - \gamma_{1_{lat}} \gamma_{0_{lat}}} = 0.7043 < 1$$

which shows that the system is stable for all choices of $0 < w_i \leq 1$. The pre-filter matrix from (37) has been designed to be $\Gamma_{lat} = \text{diag}(-0.5, -0.5)$. This may be viewed as representing the ideal response in the ϕ and the β channels. For implementation, the discontinuity in the nonlinear control term in (41) has been smoothed by using a sigmoidal approximation

$$\nu_{n,lat}^\delta = \frac{s_{lat}}{\|s_{lat}\| + \delta_{lat}}$$

where the scalar $\delta_{lat} = 0.05$ (see for example §3.7 in Edwards & Spurgeon[3]). This removes the discontinuity and introduces a further degree of tuning to accommodate the actuator rate limits – especially during actuator fault or failure conditions.

To emulate a real aircraft flight control capability, an outer loop heading control was designed based on a proportional controller plus washout filter, to provide a roll command to the inner loop sliding mode controller. In the SIMONA implementation, this outer loop heading control can be activated by a switch in the cockpit. The proportional gain was set as $K_{p_{lat}} = 0.5$ and the washout filter $\frac{s}{s+5}$ was assigned a gain $K_{w_{lat}} = 0.1$. The variables related to the adaptive nonlinear gain (§III-A1) have been chosen as $l_{1_{lat}} = 0$ and $l_{2_{lat}} = 1$. This was found to give sufficiently good performance. This removes the dependence of $r(t)$ on $x(t)$ and simplifies the implementation. The parameter η_{lat} from (25) was chosen as $\eta_{lat} = 1$. In practice, a maximum limit ρ_{max} for the adaptive nonlinear gain in (26) is imposed to avoid the actuators from becoming too aggressive. Here, the maximum

gain was set at $\rho_{max_{lat}} = 2$. The adaptation parameters from (27) have been chosen as $a_{lat} = 100$, $b_{lat} = 0.001$ and $\epsilon_{lat} = 1 \times 10^{-2}$. The parameter ϵ_{lat} was chosen to be able to tolerate the variation in $\|s_{lat}(t)\|$ due to normal changes in flight condition but small enough to enable the adaptive gain to be sensitive enough to deviation from zero due to faults or failures. Here a_{lat} has been chosen to be large to enable small changes in $\|s_{lat}(t)\|$ to cause significant changes in the gain, so that the control system reacts quickly to a fault. The parameter b_{lat} on the other hand dictates the rate at which $\rho_{lat}(t)$ will decrease, after $\|s_{lat}(t)\|$ has returned below the threshold ϵ_{lat} .

B. Longitudinal Controller Design

In normal operation, the elevators will be the primary control surface for *FPA* tracking, whilst the horizontal stabilizer introduces redundancy. For *V_{tas}* tracking, the collective thrust (from the four engines) will be the actuator. It will be assumed that at least one of the control surfaces for *FPA* tracking will still be available when a fault or failure occurs. It is also assumed that at least one of the four engines is available for *V_{tas}* tracking. Based on these assumptions, it can be verified from a numerical search that $\gamma_{0_{long}} = 8.2913$.

As in the lateral controller, a quadratic optimal design has been used to obtain the sliding surface matrix (and therefore the matrix M_{long}). The weighting matrix has been chosen as $Q_{long} = \text{diag}(0.1, 0.1, 10, 50, 1, 1)$. Again, similar to the lateral controller design, the first two terms of Q_{long} are associated with the integral action and are less heavily weighted. The third and fourth terms of Q_{long} are associated with the $B_{long,2}$ term partition in (2) (i.e. states q and V_{tas}) which weight the virtual control term, and have been heavily weighted compared to the last two terms. The poles associated with the reduced order sliding motion are $\{-0.7066, -0.2393 \pm 0.1706i, -0.0447\}$. Based on this value of M_{long} , simple calculations from (19) show that $\gamma_{1_{long}} = 1.9513 \times 10^{-4}$; therefore $\gamma_{0_{long}}\gamma_{1_{long}} = 0.0016 < 1$ and so the requirements of equation (22) are satisfied. For this choice of sliding surface, $\|G_{long}(s)\|_{\infty} = \gamma_{2_{long}} = 0.0112$ from (21). Therefore from (22),

$$\frac{\gamma_{2_{long}}\gamma_{0_{long}}}{1 - \gamma_{1_{long}}\gamma_{0_{long}}} = 0.0931 < 1$$

which shows that the system is stable for all choices of $0 < w_i \leq 1$. The pre-filter matrix from (37) has been designed to be $\Gamma_{long} = \text{diag}(-0.5, -0.125)$. The discontinuity in the nonlinear control term in (41) has been smoothed by using a sigmoidal approximation

$$v_{n,long}^{\delta} = \frac{s_{long}}{\|s_{long}\| + \delta_{long}}$$

where the scalar $\delta_{long} = 0.05$.

An outer loop altitude control scheme was designed based on a proportional controller plus washout filter to provide a *FPA* command to the inner loop sliding mode controller. In the SIMONA implementation, this outer loop altitude control can be activated by a switch in the cockpit. The proportional gain was set as $K_{p_{long}} = 0.001$ and the washout filter $\frac{s}{s+5}$ with the gain $K_{wf_{long}} = 0.05$. An adaptive nonlinear gain has been implemented. The variables related to the adaptive nonlinear gain (§III-A1) have been chosen as $l_{1_{long}} = 0$ and $l_{2_{long}} = 1$. This has been verified to give sufficiently good performance and removes the dependence of $r(t)$ on $x(t)$ which simplifies the implementation. The parameter η_{long} from (25) was chosen as $\eta_{long} = 1$. To avoid the actuators from becoming too aggressive, the maximum gain set was set at $\rho_{max_{long}} = 2$. The adaptation parameters from (27) have been chosen as $a_{long} = 100$, $b_{long} = 0.01$ and $\epsilon_{long} = 1 \times 10^{-2}$. The parameter ϵ_{long} was chosen to be able to tolerate the variation in $\|s_{long}(t)\|$ due to normal changes in flight condition but small enough to enable the adaptive gain to be sensitive enough to deviation from zero due to faults or failures. Here a_{long} has been chosen to be large to enable small changes in $\|s_{long}(t)\|$ to cause significant changes in the gain, so that the control system reacts quickly to a fault.

Note that both the lateral and longitudinal controller manipulate the engine EPRs. For lateral control, differential engine EPR is required as a secondary ‘actuator’ for β tracking; whilst for longitudinal control, collective EPR is used for *V_{tas}* tracking. In the trials, ‘control mixing’ was employed, where the signals from both the lateral controller ($e_{1_{lat}}, e_{2_{lat}}, e_{3_{lat}}$ and $e_{4_{lat}}$) and longitudinal controller ($e_{1_{long}}, e_{2_{long}}, e_{3_{long}}$ and $e_{4_{long}}$) were added together before being applied to the engines (page 14 of Burcham *et al.*[36]). This is similar to the control strategy used for the NASA propulsion control aircraft described in Burcham *et al.*[36].

Remark 6: In terms of the control laws no actuator magnitude or rate saturations are accounted for explicitly – although in the evaluations on SIMONA these effects are present. However, if a rate limit or position limit is

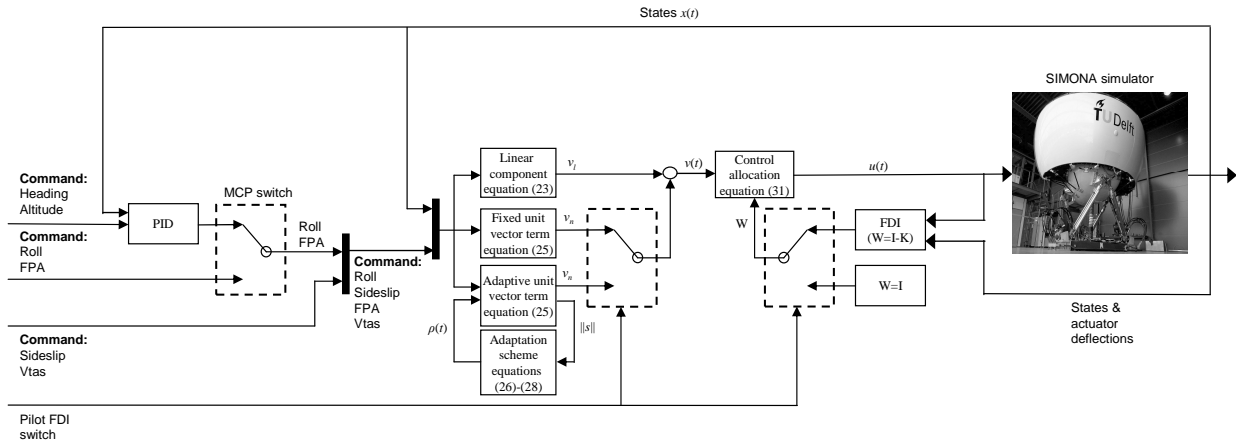


Fig. 2. SIMONA interconnections



Fig. 3. Mode control panel (MCP)

exceeded, a difference between the expected actuator position and the commanded one occurs which would be interpreted as a ‘fault’. The proposed scheme would then inherently attempt to reduce the burden in this channel and redistribute the control effort to other actuators, which would mitigate the effect of the saturation.

V. RESULTS FROM THE SIMONA IMPLEMENTATIONS

The results presented in this paper are all from the 6-DOF SIMONA simulator. The controllers have been implemented as SIMULINK (version 2006b) models with appropriate inputs and outputs to connect with the aircraft model and the SIMONA hardware. Figure 2 gives a schematic of the overall control architecture and its connections with the SIMONA hardware. The controllers employ an Ode4 solver with a fixed time step of 0.01s. Using the Real-Time Workshop, the SIMULINK controller block diagrams were converted to C-code and integrated into the SRS, where they run in real-time on a dual Pentium III 1 GHz processor within the allowed 10 ms update frame.

A connection with the Mode Control Panel on the flight deck (Figure 3) enables the selection of ‘control modes’ e.g. altitude hold, heading select and reference values. The pilot commands new headings, speeds or altitudes by adjusting the controls on the MCP.

For passenger comfort during turning manoeuvres, the reference command for ϕ was limited to 25deg and a 0deg reference applied to β to force slide-slip free flight. It was assumed that the aircraft has recently taken off and reached an altitude of 600m. After a few seconds of straight and level flight, failures occur on the actuators. The immediate action requested by the pilot is to change the heading to 180deg and to head back to the runway. The altitude is then changed from 600m (1967.2ft) to 30.5m (100ft) before the V_{tas} is reduced from 92.8m/s(180kn) to 82.3m/s(160kn), to approximate a landing manoeuvre. For clarity and reproducibility, no measurement noise was introduced to the signals used in the controller calculations.

Five different control surface failures have been tested on the simulator: all elevators jam with a 3deg offset, all ailerons jam with a 3deg offset, a stabilizer runaway, all rudders runaway and finally both rudders detach from the vertical fin [9]. All the trials have been done with and without fault detection, isolation and estimation (FDI), and with and without wind and turbulence. However due to space limitations, only the most significant results are shown in this paper. The results from two distinct controllers will be presented: the results from the adaptive gain

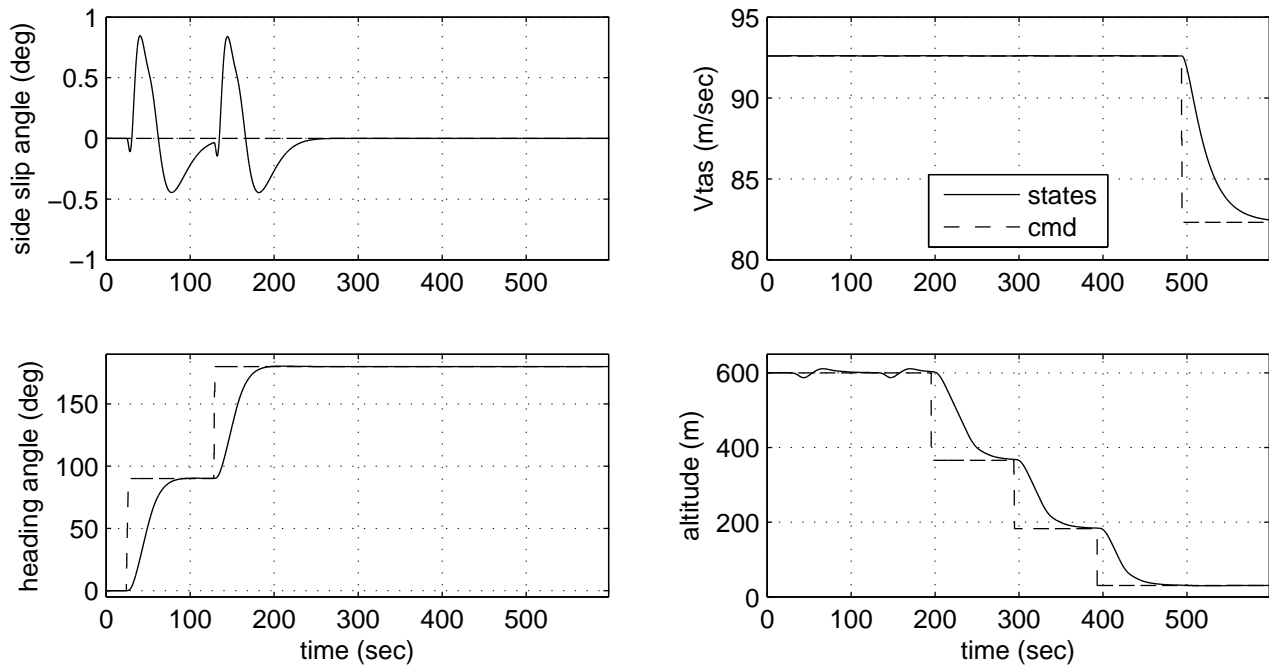


Fig. 4. no fault condition: controlled states

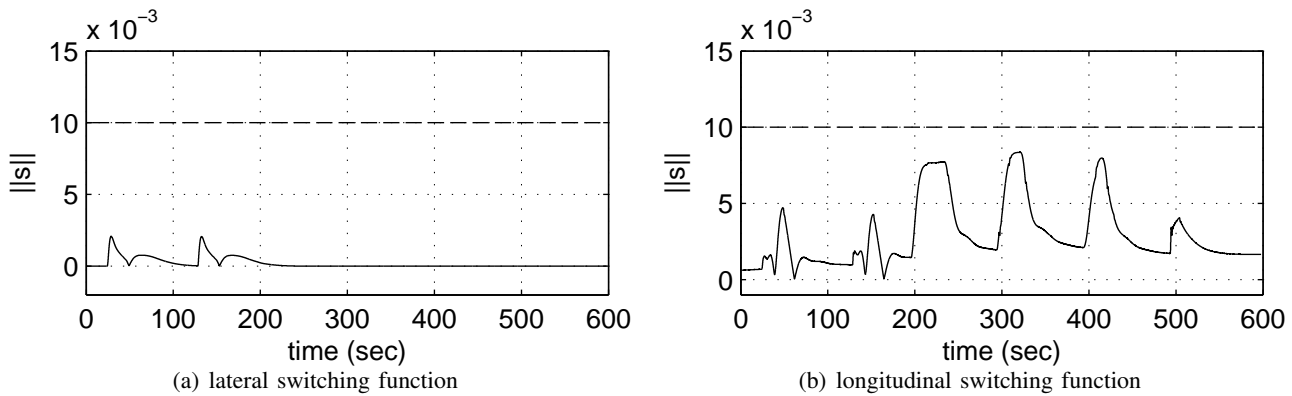


Fig. 5. no fault condition, FDI off

scheme proposed earlier in the paper in §III; and also results from a more complex scheme proposed by Alwi & Edwards[8].

Figures 4-6 show the fault-free responses of the controller. Figure 4 shows that there is a small amount of coupling between roll and sideslip during a heading change. There is also a small change in altitude during heading change. The heading is changed by means of two 90deg step inputs followed by a change in altitude from 600m to 30m in 3 steps: 600m to 366m to 183m and finally to 30m above the runway. Figure 4 shows good tracking by the states of the command signals. Figure 5 shows the nominal variation in the norm of the switching function signals for the longitudinal and lateral controller. Finally figure 6 shows the overall trajectory of the aircraft in 3D. Here, the change in heading and altitude can be seen more clearly.

A. Fixed Control Allocation

This subsection presents implementation results from the adaptive gain scheme proposed earlier in §III. No explicit FDI is required and the strong robustness properties of the sliding mode control allocation scheme are exploited to achieve *passive* fault tolerant control.

Figures 7-9 show the responses when all ailerons become jammed with an offset of 3deg (figure 8) after 6.3sec

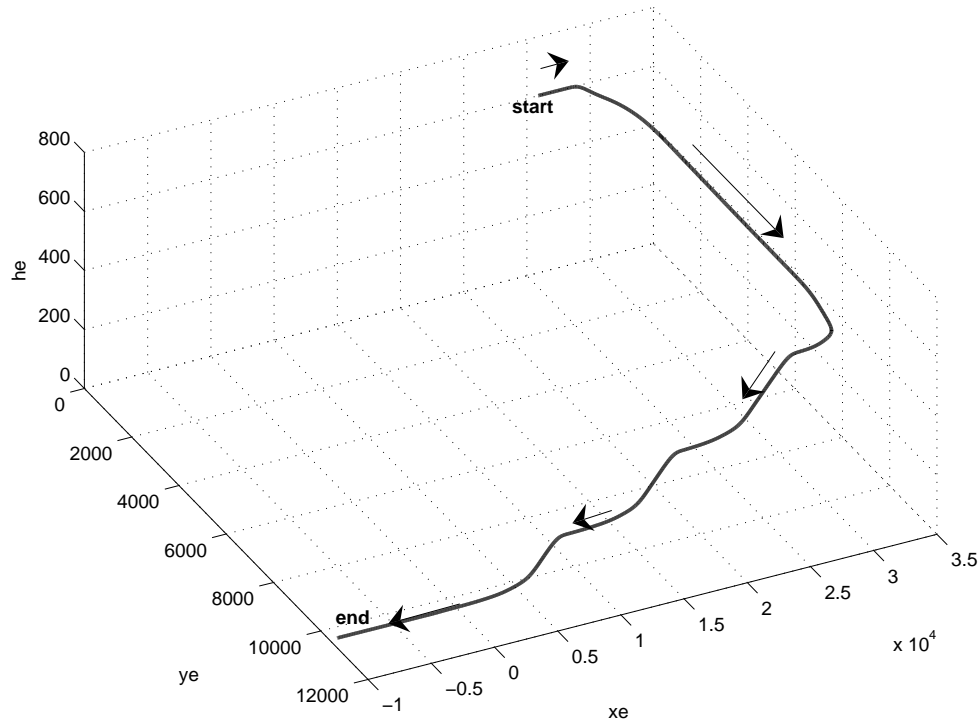


Fig. 6. no fault condition: flight trajectory

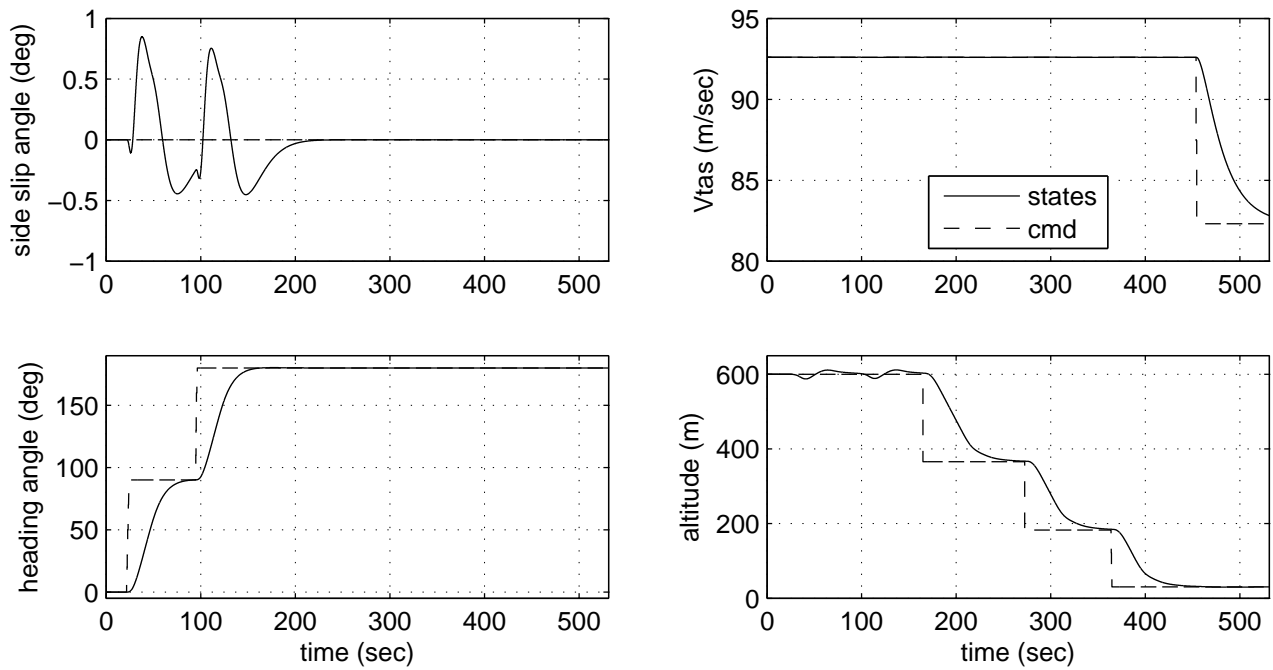


Fig. 7. aileron jam with offset, FDI off: controlled states

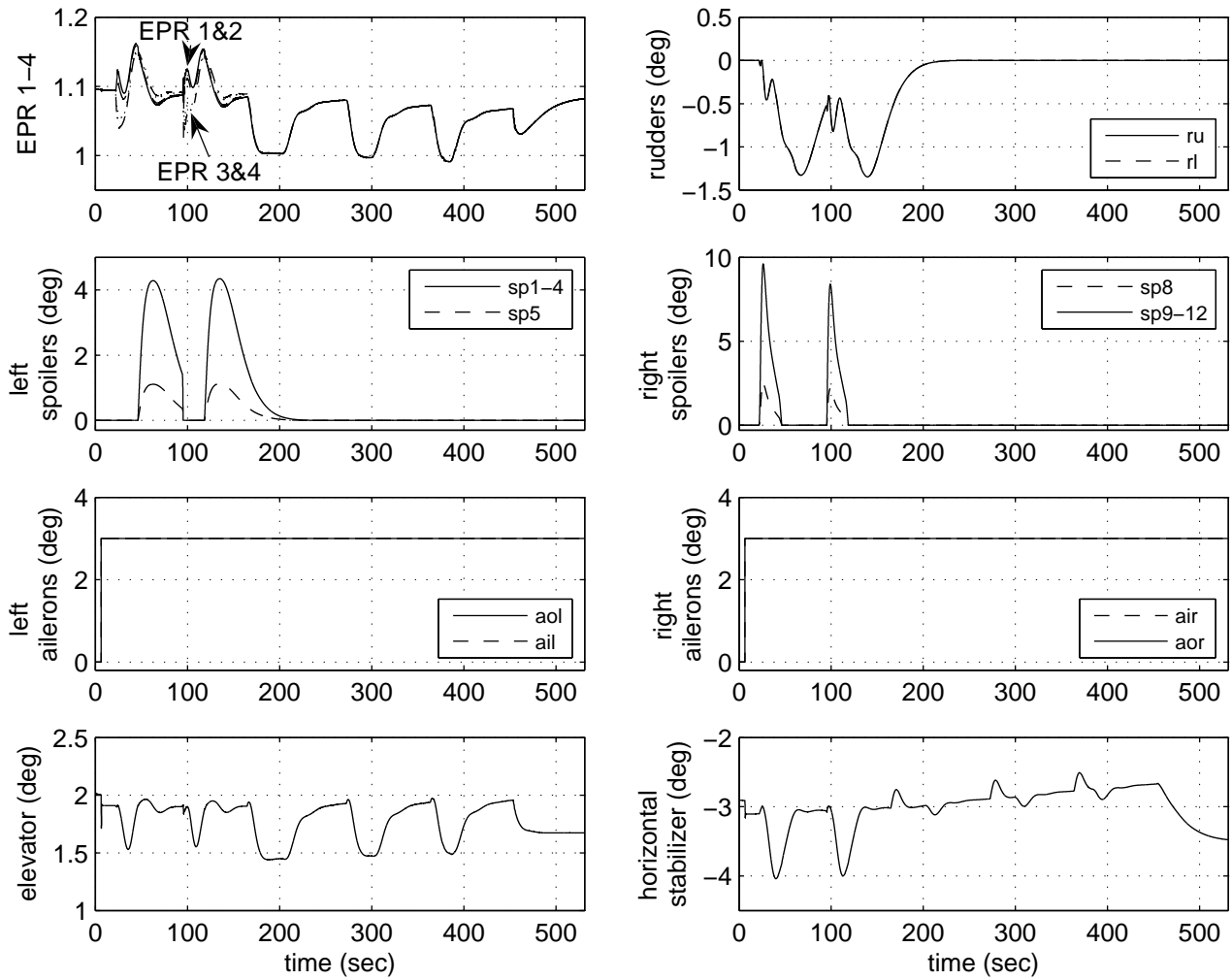


Fig. 8. aileron jam with offset, FDI off: actuator positions

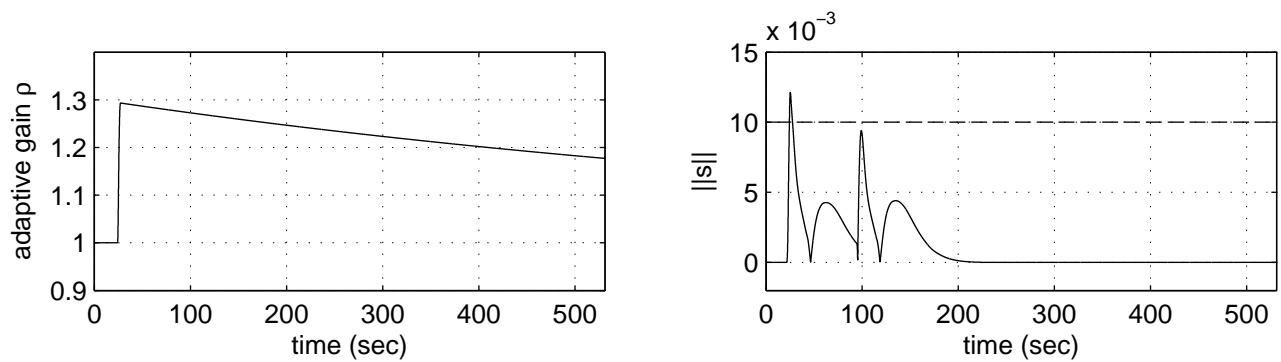


Fig. 9. aileron jam with offset, FDI off: lateral adaptive gain & switching function

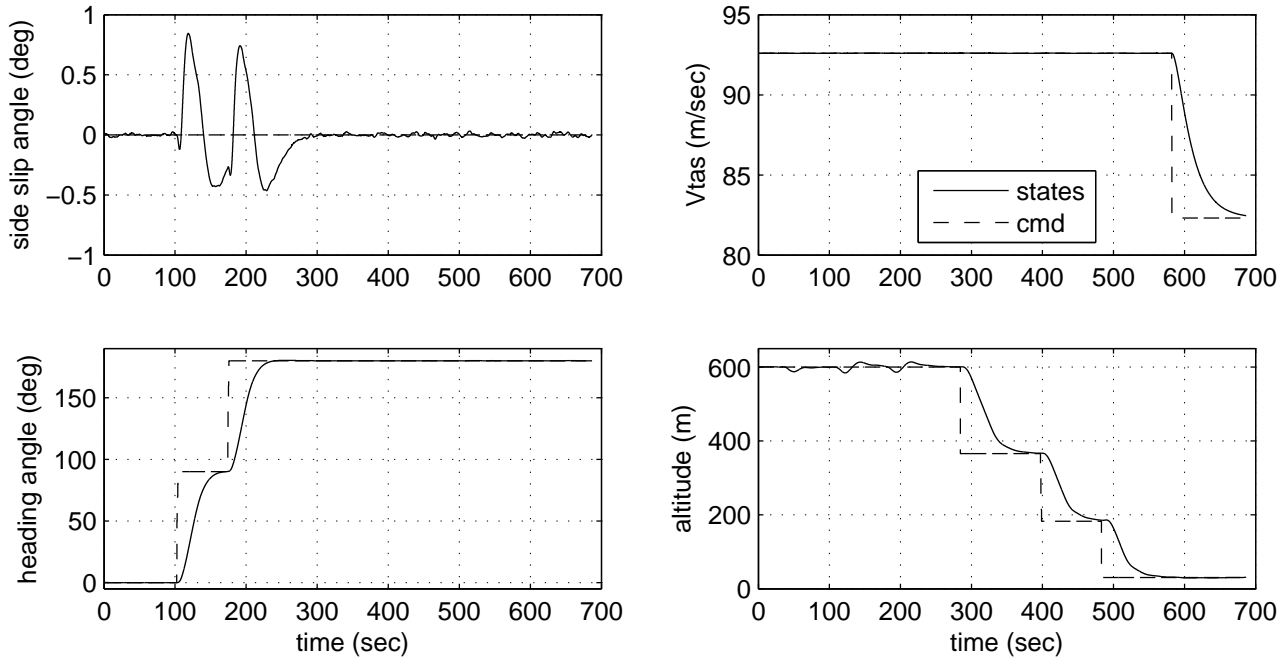


Fig. 10. stabilizer runaway with wind & gust, FDI off: controlled states

in straight and level flight. Figure 8 shows that the spoilers become more active compared to the no fault condition. (Note: in figure 8, ru: upper rudder, rl: lower rudder, sp: spoilers, aol: left outer aileron, ail: left inner aileron, air: right inner aileron and aor: outer right aileron). Figure 9 shows that due to the abrupt offset of 3deg during the jam failure, the lateral switching function temporarily exceeds the threshold ϵ_{lat} and this triggers the adaptive mechanism which increases the gain $\rho(t)$. However the switching function never exceeds this threshold again and the lateral adaptive gain gradually begins to decrease. Figure 7 shows no degradation in performance of the controlled states compared to the nominal condition.

Figures 10-12 show responses dealing with a stabilizer runaway in the presence of wind and gusts. Figure 11 shows that the stabilizer has moved at its maximum deflection rate to its maximum deflection of 3deg. This is quite a catastrophic failure as this deflection causes the aircraft to pitch down suddenly. Figure 12 indicates the severity of the stabilizer runaway failure since the switching function exceeds and stays outside the threshold and the adaptive gain reaches its maximum value. Figure 11 shows that the elevator reacts to the failure and begins to counteract the effect of the stabilizer runaway. Figure 10 shows only a small degradation in performance compared to the nominal fault free condition.

B. On-line Control Allocation

In this subsection, the implementation results of an earlier sliding mode control allocation scheme proposed by Alwi & Edwards[8] will be presented. The only significant difference between this one and the scheme proposed in §III is that the control law is now given by

$$u(t) = WB_2^T(B_2W^2B_2^T)^{-1}\hat{v}(t)$$

This control law arises from choosing the weighting matrix Ω in (12) as the efficiency measure W . However in order to implement this control law, information about the w_i that comprise the diagonal elements of W must be available online. This therefore requires a FDI scheme – or more specifically, a fault estimation scheme. In this paper, it will be assumed that a measurement of the actual actuator deflection is available. This is not an unrealistic assumption in aircraft systems. Information provided by the actual actuator deflection can be compared with the signals from the controller to indicate the effectiveness of the actuator. This therefore constitutes an FDI scheme and incurs additional computational overhead in terms of the online implementation. The idea is to use a ‘least

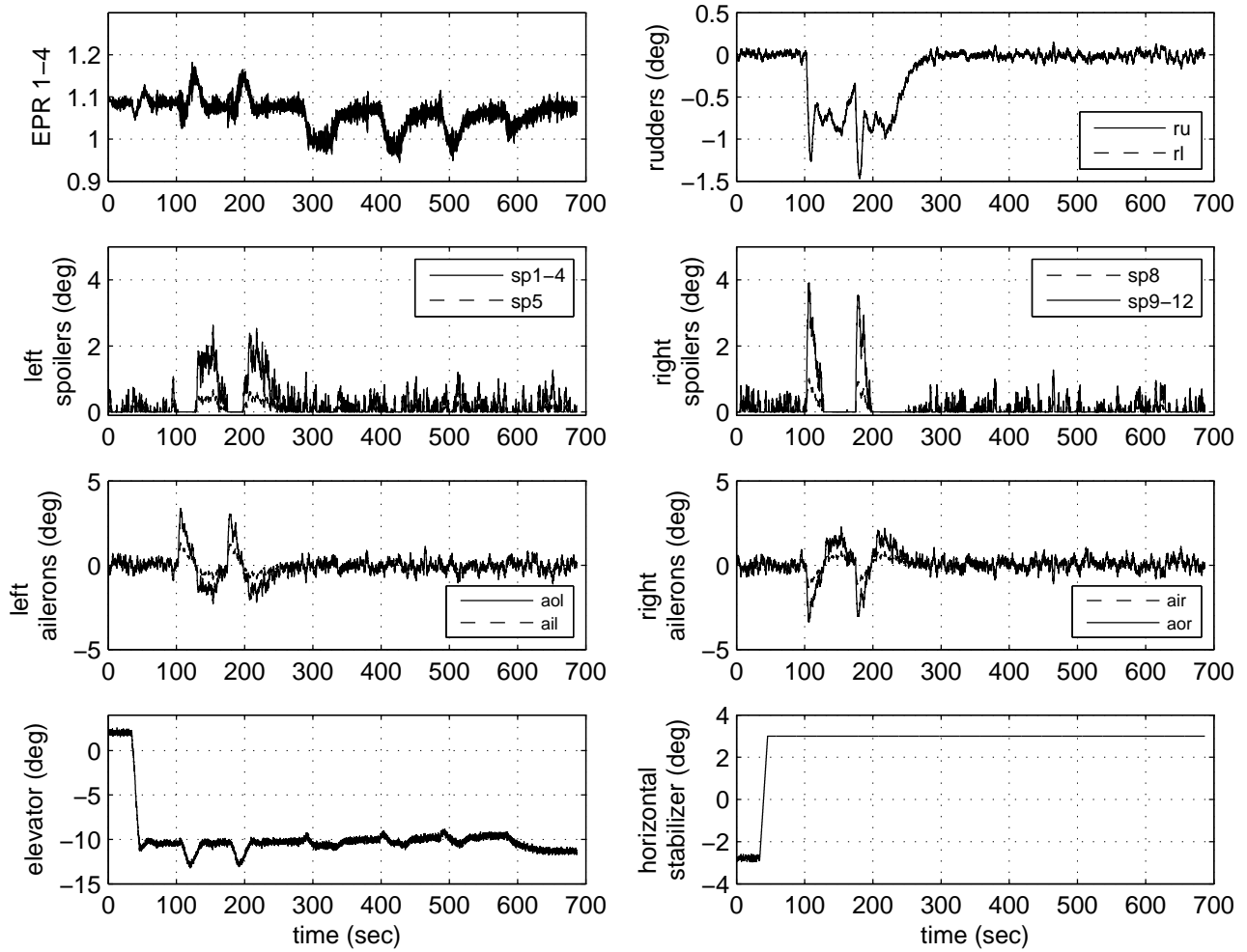


Fig. 11. stabilizer runaway with wind & gust, FDI off: actuator positions

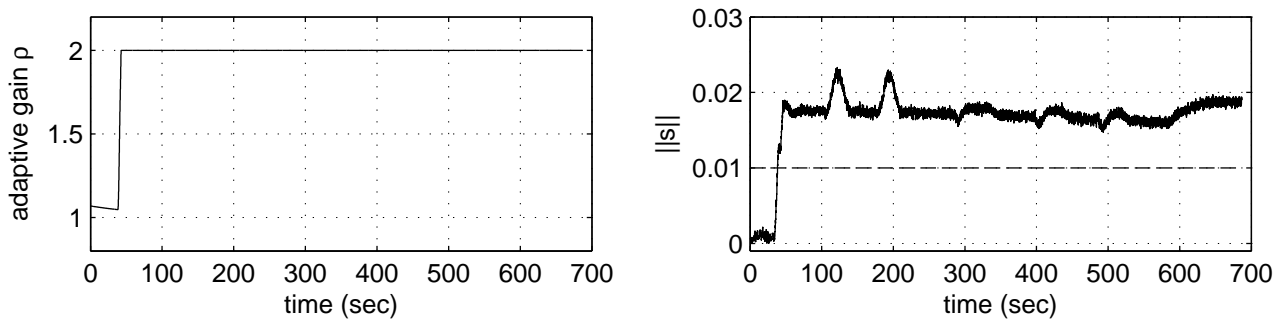


Fig. 12. stabilizer runaway with wind & gust, FDI off: longitudinal adaptive gain & switching function

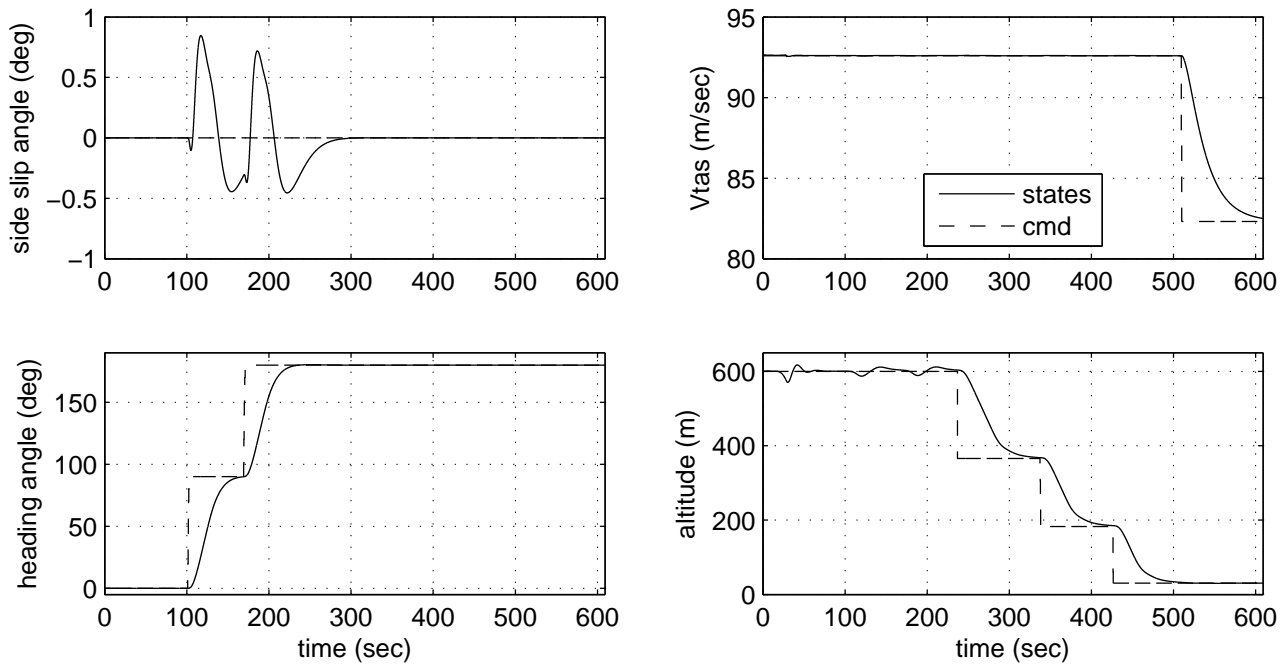


Fig. 13. stabilizer runaway, FDI on: controlled states

squares' method to estimate the coefficients w_i and c_i in a relationship of the form

$$u_{(i,a)} = w_i u_i + c_i$$

where $u_{(i,a)}$ represents the actual deflection and u_i represents the demanded deflection i.e. the controller output. The scalars w_i and c_i can be obtained from a least squares optimization and $W := \text{diag}(w_1, \dots, w_m)$. If the i th actuator is working perfectly, $w_i = 1$ and $c_i = 0$. If $w_i < 1$ then a fault is present. In the SIMONA implementation, 10 data samples from a 'moving window', collected at 100Hz are used to compute the w_i and c_i . In the SIMONA implementation, both the lateral and longitudinal controller has its own fault estimation block based on the control surfaces to be controlled.

Figures 13-15 show a stabilizer runaway failure. Figure 13 shows no visible degradation in performance. The switching function shown in Figure 15, exceeds the threshold briefly after the failure, but immediately returns inside the threshold. Compared to Figure 12, the on-line allocation scheme with only a fixed nonlinear gain ($\rho_{long} = 1$) has maintained the switching function below the threshold. This shows the advantage of using the on-line control allocation scheme when information about the effectiveness of the control surface is available. Figure 15 shows that the effectiveness of the stabilizer has been successfully estimated and this information has been used to provide on-line control allocation.

Figures 16-18 show the responses for a rudder runaway. Figure 17 shows that the upper and lower rudders runaway to the 5deg position. This is the hardest situation to control. Not only does the rudders runaway cause a tendency to turn to one side (and therefore affecting the lateral performance), it also creates difficulties in the longitudinal axis and results in a tendency to pitch up. Figure 16 shows that the controller is tested on a slightly different manoeuvre. The sideslip command is kept at 0deg and has only small degradation in its performance. The heading is changed by 180deg by banking to the right and at the same time the speed is increased to 113.18m/s (220kn) adding further difficulties to the banking manoeuvre. Then a bank left is tested by changing the demanded heading back to 135deg, followed by a reduction in speed to 92.6m/s. The altitude is also decreased to 30m, before a small increase in altitude to 182m above the runway. In these tests, only a small degradation in performance is visible. Figure 18 shows that the switching function just exceeds the threshold at high speed indicating that at higher speed, the effect of the rudder runaway is harder to control. However, using the rudder effectiveness information in Figure 18 the control signal sent to the rudder is shut-off and the control signals are sent to the remaining functioning actuators causing a visible split in the control surface deflections seen in Figure 17. Figure 17 shows

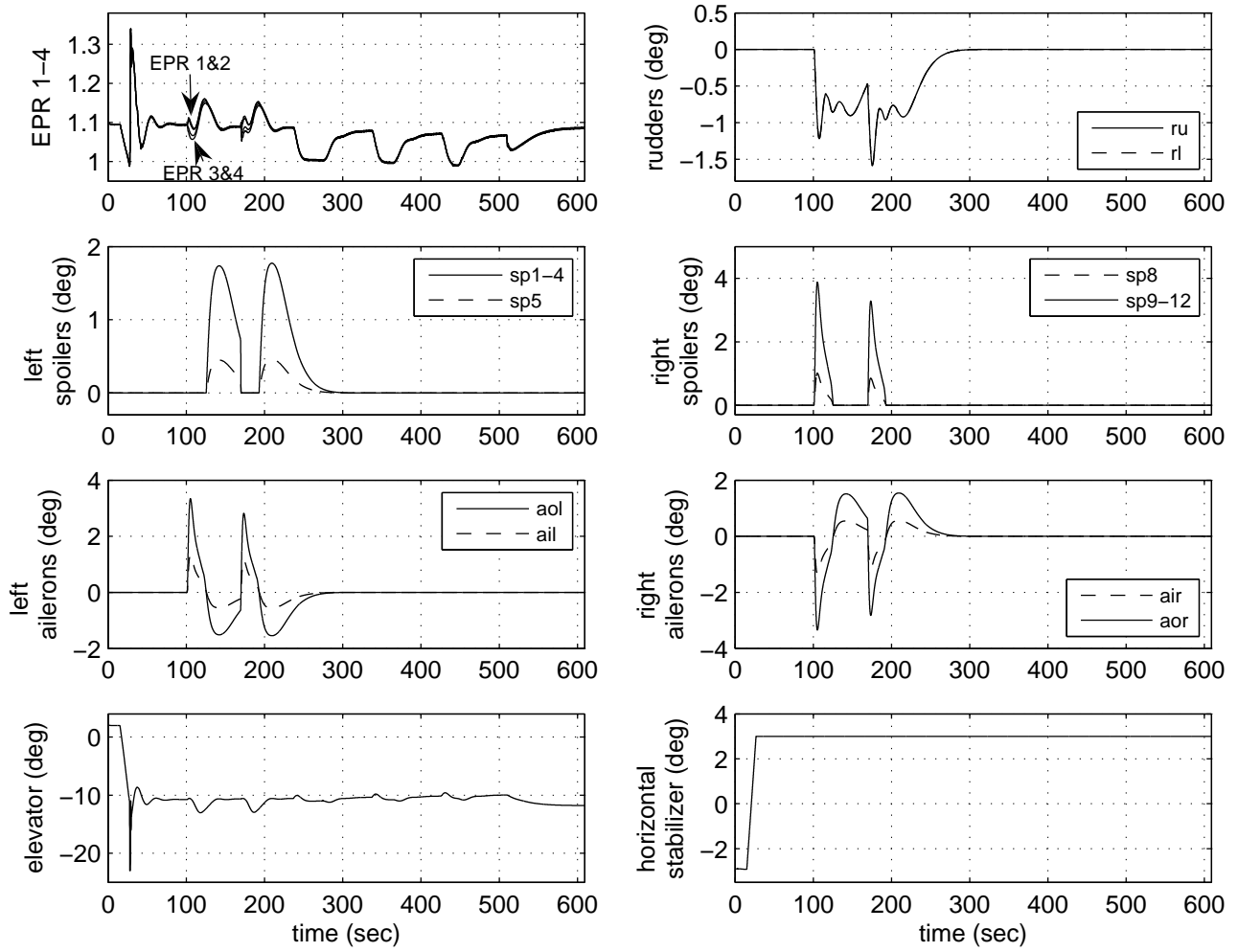


Fig. 14. stabilizer runaway, FDI on: actuator positions

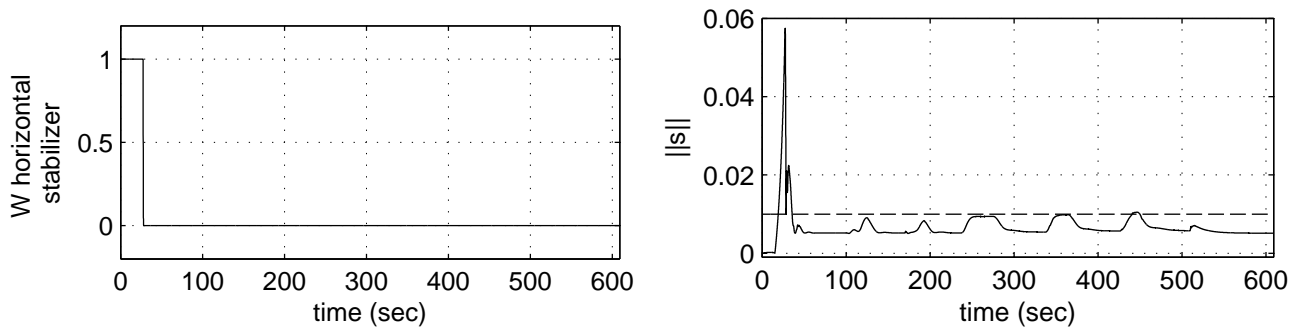


Fig. 15. stabilizer runaway, FDI on: stabilizer effectiveness and longitudinal switching function

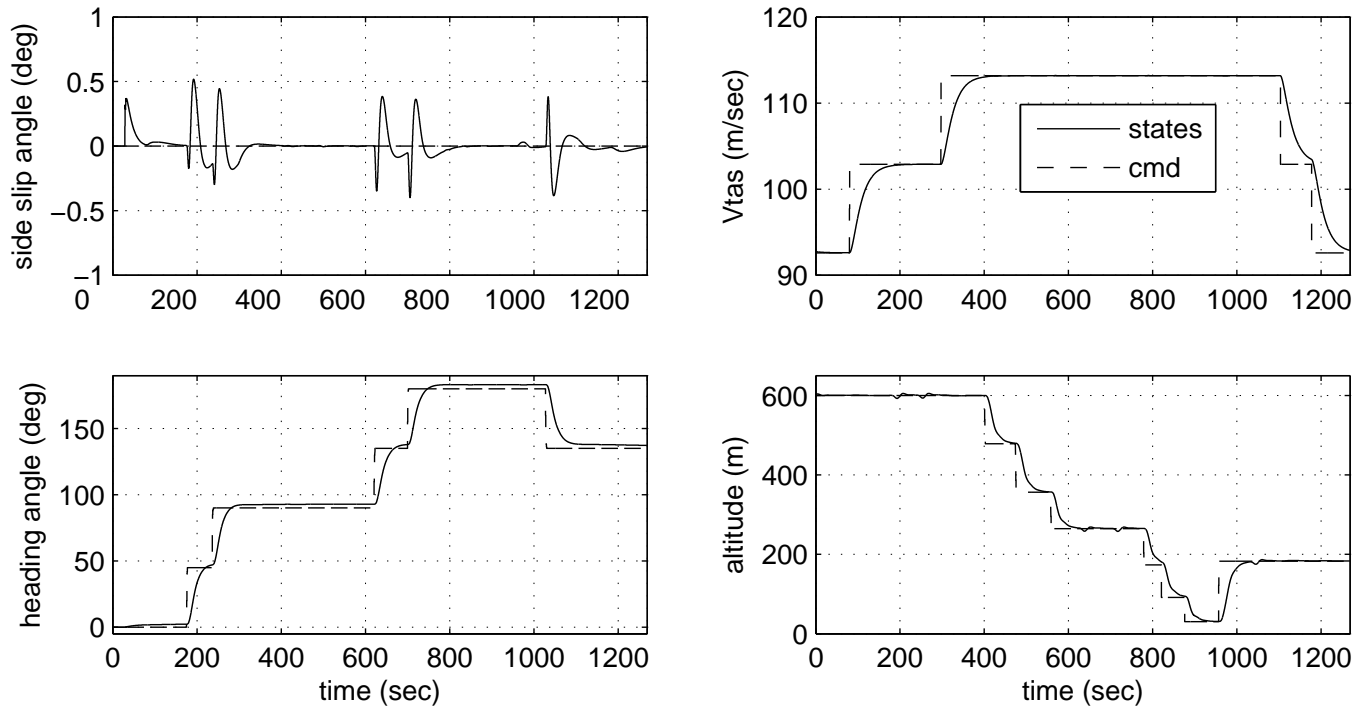


Fig. 16. rudder runaway, FDI on: controlled states

the 4 engine pressure ratios (EPR) have split to counteract the effect of the banking turn to the left. Engine 3 and 4 on the right wing show less EPR compared to Engine 1 and 2 on the left wing to counteract the tendency to turn to the left. The spoilers and ailerons also show a visible split in terms of the deflections to counteract the effect of the rudder runaway.

VI. CONCLUSIONS

This paper has presented sliding mode control allocation schemes for fault tolerant control. The control allocation aspect is used to allow the sliding mode controller to redistribute the control signals to the remaining functioning actuators when a fault or failure occurs, without reconfiguring or switching to another controller. This paper has provided a rigorous analysis of the proposed sliding mode control allocation scheme and has determined the nonlinear gain required to maintain sliding. The two schemes, implemented on the SIMONA research flight simulator have shown good performance not only in nominal conditions, but also in the case of total actuator failures, even in wind and gust conditions.

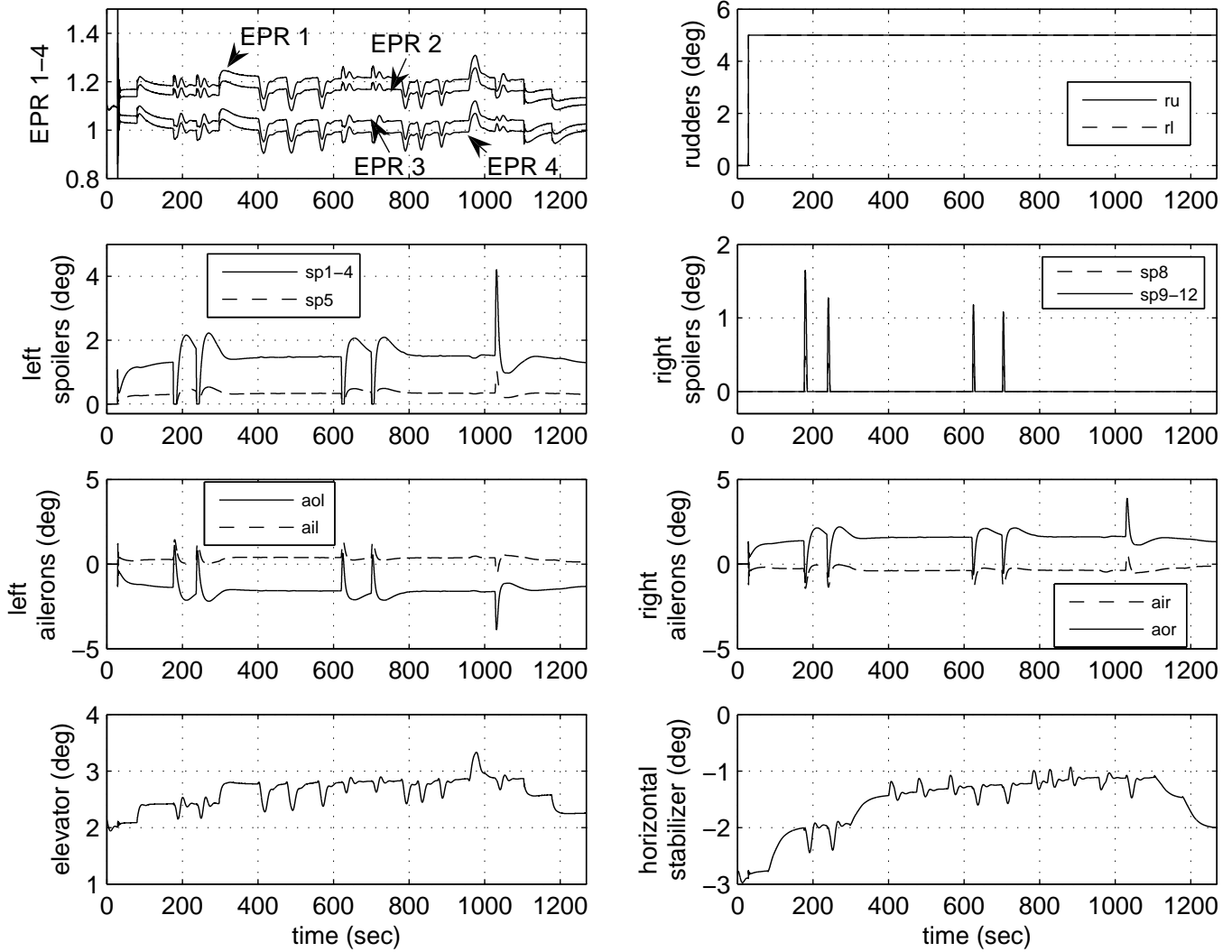


Fig. 17. rudder runaway, FDI on: actuator positions

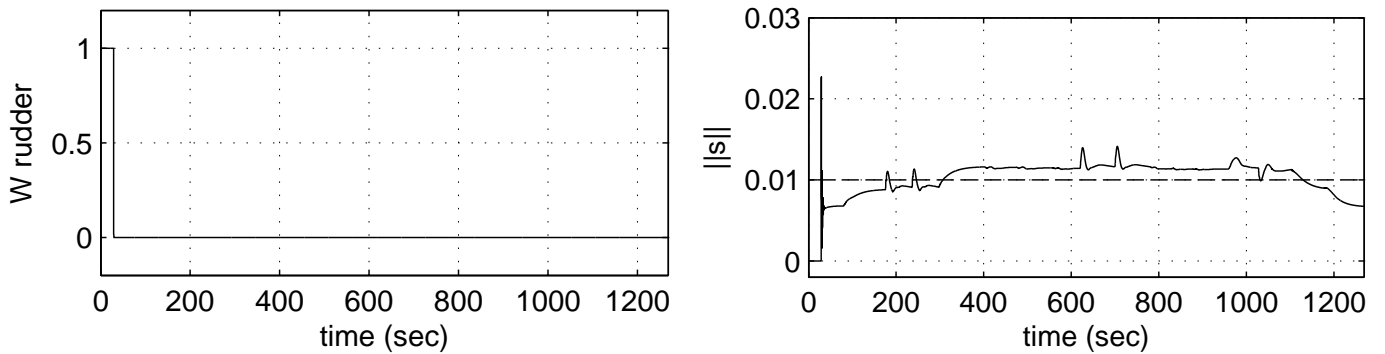


Fig. 18. rudder runaway, FDI on: rudder effectiveness and lateral switching function

REFERENCES

- [1] J. Buffington, P. Chandler, M. Pachter, On-line system identification for aircraft with distributed control effectors, *International Journal of Robust and Nonlinear Control* 9 (1999) 1033–1049.
- [2] J. B. Davidson, F. J. Lallman, W. T. Bundick, Real-time adaptive control allocation applied to a high performance aircraft, in: 5th SIAM Conference on Control & Its Application, 2001.
- [3] C. Edwards, S. Spurgeon, *Sliding Mode Control: Theory and Applications*, Taylor & Francis, 1998.
- [4] Y. Shtessel, J. Buffington, S. Banda, Tailless aircraft flight control using multiple time scale re-configurable sliding modes, *IEEE Transactions on Control Systems Technology* 10 (2002) 288–296.
- [5] S. R. Wells, R. A. Hess, Multi-input/multi-output sliding mode control for a tailless fighter aircraft, *Journal of Guidance, Control and Dynamics* 26 (2003) 463–473.
- [6] D. Shin, G. Moon, Y. Kim, Design of reconfigurable flight control system using adaptive sliding mode control: actuator fault, *Proceedings of the Institution of Mechanical Engineers, Part G (Journal of Aerospace Engineering)* 219 (2005) 321–328.
- [7] M. L. Corradini, G. Orlando, G. Parlangeli, A fault tolerant sliding mode controller for accommodating actuator failures, in: 44th IEEE Conference on Decision and Control, 2005.
- [8] H. Alwi, C. Edwards, Sliding mode FTC with on-line control allocation, in: 45th IEEE Conference on Decision and Control, 2006.
- [9] M. H. Smaili, J. Breeman, T. J. J. Lombaerts, D. A. Joosten, A simulation benchmark for integrated fault tolerant flight control evaluation, in: AIAA Modeling and Simulation Technologies Conference and Exhibit, 2006.
- [10] A. Marcos, G. Balas, A Boeing 747–100/200 aircraft fault tolerant and diagnostic benchmark, Tech. Rep. AEM–UoM–2003–1, Department of Aerospace and Engineering Mechanics, University of Minnesota (2003).
- [11] C. A. A. M. van der Linden, DASMAT: Delft university aircraft simulation model and analysis tool, Tech. Rep. LR–781, Technical University of Delft, The Netherlands (1996).
- [12] M. Smaili, Flightlab 747: Benchmark for advance flight control engineering, Tech. rep., Technical University Delft, The Netherlands (1999).
- [13] A. Marcos, S. Ganguli, G. Balas, An application of H_∞ fault detection and isolation to a transport aircraft, *Control Engineering Practice* 13 (2005) 105–119.
- [14] I. Szaszi, A. Marcos, G. J. Balas, J. Bokor, Linear parameter-varying detection filter design for a Boeing 747-100/200 aircraft, *Journal of Guidance, Control, and Dynamics* 28 (2005) 461–470.
- [15] J. M. Maciejowski, C. N. Jones, MPC fault-tolerant control case study: flight 1862, in: Proceedings of the IFAC Symposium SAFEPROCESS 03, Washington, 2003.
- [16] O. Stroosma, M. M. van Paassen, M. Mulder, Using the simona research simulator for human-machine interaction research, in: AIAA Modeling and Simulation Technologies Conference, 2003.
- [17] H. M. Heerspink, W. R. Berkouwer, O. Stroosma, M. M. van Paassen, M. Mulder, J. Mulder, Evaluation of vestibular thresholds for motion detection in the simona research simulator, in: AIAA Modeling and Simulation Technologies Conference, 2005.
- [18] A. R. Valente Pais, M. Mulder, M. M. Van Paassen, M. Wentink, E. Groen, Modeling human perceptual thresholds in self-motion perception, in: AIAA Modeling and Simulation Technologies Conference, 2006.
- [19] P. M. T. Zaal, F. M. Nieuwenhuizen, M. M. M. M. Van Paassen, Perception of visual and motion cues during control of self-motion in optic flow environments, in: AIAA Modeling and Simulation Technologies Conference, 2006.
- [20] B. Gouverneur, J. A. B. Mulder, M. M. R. van Paassen, O. Stroosma, Optimization of the simona research simulator's motion filter settings for handling qualities experiments, in: AIAA Modeling and Simulation Technologies Conference and Exhibit, 2003.
- [21] E. J. Field, T. R. Pinney, M. R. van Paassen, O. S. R. A. Rivers, Effects of implementation variations on the results of piloted simulator handling qualities evaluations, in: AIAA Modeling and Simulation Technologies Conference and Exhibit, 2004.
- [22] T. M. Lam, M. Mulder, M. M. Van Paassen, J. A. Mulder, Comparison of control and display augmentation for perspective flight-path displays, *Journal of Guidance, Control, and Dynamics* 29 (2006) 564–578.
- [23] M. Mulder, A. R. Veldhuijzen, M. M. Van Paassen, J. Mulder, Integrating fly-by-wire controls with perspective flight-path displays, *Journal of Guidance, Control, and Dynamics* 28 (2005) 1263–74.
- [24] W. F. De Gaay Fortman, M. M. Van Paassen, M. Mulder, A. C. In 't Veld, J. P. Clarke, Implementing time-based spacing for decelerating approaches, *Journal of Aircraft* 44 (2007) 106–118.
- [25] J. L. De Prins, F. K. M. Schippers, M. Mulder, M. M. Van Paassen, A. C. In 't Veld, J. P. Clarke, Enhanced self-spacing algorithm for three-degree decelerating approaches, *Journal of Guidance, Control, and Dynamics* 30 (2007) 576–90.
- [26] F. J. Vormer, M. Mulder, M. M. Van Paassen, J. A. Mulder, Optimization of flexible approach trajectories using a genetic algorithm, *Journal of Aircraft* 43 (2006) 941–52.
- [27] J. D. Boskovic, R. K. Mehra, Control allocation in overactuated aircraft under position and rate limiting, in: Proceedings of the American Control Conference, 2002, pp. 791–796.
- [28] O. Härkegård, S. T. Glad, Resolving actuator redundancy - optimal control vs. control allocation, *Automatica* 41 (2005) 137–144.
- [29] R. Patton, Robustness in model-based fault diagnosis: the 1997 situation, *IFAC Annual Reviews* 21 (1997) 101–121.
- [30] J. X. Xu, Q. W. Jia, T. H. Lee, On the design of a nonlinear adaptive variable structure derivative estimator, *IEEE Transactions on Automatic Control* 45 (2000) 1028–1033.
- [31] G. Wheeler, C. Su, Y. Stepanenko, Sliding mode controller with improved adaptation laws for the upper bounds on the norm of uncertainties, *Automatica* 34 (1998) 1657–1661.
- [32] C. Tan, C. Edwards, Sliding mode observers for robust detection and reconstruction of actuator and sensor faults, *International Journal of Robust and Nonlinear Control* 13 (2003) 443–463.
- [33] A. E. Bryson, *Control of spacecraft and aircraft*, Princeton University Press, 1994.
- [34] S. Ganguli, A. Marcos, G. Balas, Reconfigurable LPV control design for Boeing 747-100/200 longitudinal axis, in: American Control Conference, 2002, pp. 3612–3617.
- [35] V. Utkin, *Sliding Modes in Control Optimization*, Springer-Verlag, Berlin, 1992.

- [36] F. W. Burcham, T. A. Maine, J. Kaneshinge, J. Bull, Simulator evaluation of simplified propulsion-only emergency flight control system on transport aircraft, Tech. Rep. NASA/TM-1999-206578, NASA (1999).

APPENDIX

Proof of Proposition 1: Define a scalar

$$\zeta := \frac{(2 + \gamma_1)}{w^2(1 - \gamma_1\gamma_0)} \quad (43)$$

The expression for ζ in (43) is guaranteed to be positive, since in the requirements of equation (22), the inequality $\gamma_1\gamma_0 < 1$ must hold. Assume that $\dot{K}(t) = 0$ almost always, this implies $\dot{W}(t) = 0$ almost always and so only isolated abrupt step changes in the effectiveness are considered here. Using the fact that $(B_2WB_2^T) > 0$ for all $w \in \mathcal{W}$, the following candidate Lyapunov function

$$V = \frac{1}{2} \left(s^T(B_2WB_2^T)s + \frac{1}{a} \lambda(B_2WB_2^T)^2(1 - \gamma_1\gamma_0)(r(t) - \zeta)^2 \right) \quad (44)$$

where a is the positive scalar from (27), is positive definite with respect to s , the adaptive gain error $r(t) - \zeta$, and is radially unbounded. Taking derivatives along trajectories

$$\dot{V} = s^T(B_2WB_2^T)\dot{s} + \frac{1}{a} \lambda(B_2WB_2^T)^2(1 - \gamma_1\gamma_0)(r(t) - \zeta)\dot{r}(t) \quad (45)$$

where from (17),

$$\begin{aligned} \dot{s}(t) &= \tilde{A}_{21}\hat{x}_1(t) + \tilde{A}_{22}s(t) + \nu(t) - (I - MB_1B_2^NWB_2^T - B_2WB_2^T)\nu(t) \\ &= (I + MB_1B_2^NB_2^+)(B_2WB_2^T)\nu_n(t) - (I - MB_1B_2^NWB_2^T - B_2WB_2^T)\nu_l(t) \end{aligned}$$

Using the fact that $s(t)^T(B_2WB_2^T)(B_2WB_2^T)s(t) = \|B_2WB_2^T s\|^2$ where $\|(B_2WB_2^T)\| \leq \|B_2B_2^T\| = 1$, and $\|WB_2^T\| \leq \|W\|\|B_2^T\| \leq 1$ for all $(w_1, \dots, w_m) \in \mathcal{W}$, it follows that when $s \neq 0$

$$\begin{aligned} s^T(B_2WB_2^T)\dot{s} &= -\frac{(\rho + \eta)}{\|s\|} \|B_2WB_2^T s\|^2 - (\rho + \eta)s^T(B_2WB_2^T)(MB_1B_2^NB_2^+)(B_2WB_2^T) \frac{s}{\|s\|} \\ &\quad - s^T(B_2WB_2^T)(I - MB_1B_2^NWB_2^T - B_2WB_2^T)\nu_l(t) \\ &\leq -\frac{(\rho + \eta)}{\|s\|} \|B_2WB_2^T s\|^2 + \frac{(\rho + \eta)}{\|s\|} \|B_2WB_2^T s\|^2 \|(MB_1B_2^NB_2^+)\| \\ &\quad + \|B_2WB_2^T s\| \|(I - MB_1B_2^NWB_2^T - B_2WB_2^T)\| \|\nu_l(t)\| \\ &\leq \|B_2WB_2^T s\| \left(-\frac{(\rho + \eta)}{\|s\|} \|B_2WB_2^T s\| (1 - \gamma_1\gamma_0) + (2 + \gamma_1) \|\nu_l(t)\| \right) \end{aligned} \quad (46)$$

since $\|MB_1B_2^NB_2^+\| \leq \|MB_1B_2^N\| \|B_2^+\| \leq \gamma_0\gamma_1$, and

$$\|I - MB_1B_2^NWB_2^T - B_2WB_2^T\| \leq 1 + \|MB_1B_2^NWB_2^T\| + \|B_2WB_2^T\| \leq 2 + \gamma_1$$

Using the Rayleigh principle, $-\|B_2WB_2^T s\|^2 \leq -\lambda(B_2WB_2^T)^2 \|s\|^2 \leq -w^2 \|s\|^2$, and using the fact that $\bar{\lambda}(B_2WB_2^T) = 1$, inequality (46) implies

$$\begin{aligned} s^T(B_2WB_2^T)\dot{s} &\leq -w^2 \|s\| (\rho + \eta) (1 - \gamma_1\gamma_0) + \|s\| (2 + \gamma_1) \|\nu_l(t)\| \\ &= w^2 \|s\| (1 - \gamma_1\gamma_0) \left(-(\rho + \eta) + \zeta \|\nu_l(t)\| \right) \end{aligned} \quad (47)$$

where ζ is defined in (43). Using (24) and (26), the inequality above can be written as

$$s^T(B_2WB_2^T)\dot{s} \leq -w^2 \|s\| (1 - \gamma_1\gamma_0) \eta - w^2 \|s\| (1 - \gamma_1\gamma_0) (l_1 \|x(t)\| + l_2) (r(t) - \zeta) \quad (48)$$

Finally, substituting (27) and (48) into (45) yields

$$\begin{aligned} \dot{V} &\leq -w^2 \|s\| (1 - \gamma_1\gamma_0) \eta - w^2 \|s\| (1 - \gamma_1\gamma_0) (l_1 \|x(t)\| + l_2) (r(t) - \zeta) \\ &\quad + w^2 (1 - \gamma_1\gamma_0) (r(t) - \zeta) (l_1 \|x(t)\| + l_2) D_\epsilon(\|s(t)\|) \\ &\quad - \frac{b}{a} w^2 (1 - \gamma_1\gamma_0) (r(t) - \zeta) r(t) \end{aligned} \quad (49)$$

If $\|s\| > \epsilon$ then $D_\epsilon(\|s\|) = \|s\|$ and so substituting in (49) and simplifying terms yields

$$\dot{V} \leq -w^2\|s\|(1 - \gamma_1\gamma_0)\eta - \frac{b}{a}w^2(1 - \gamma_1\gamma_0)(r(t) - \zeta)r(t) \quad (50)$$

By construction $0 \leq \gamma_1\gamma_0 < 1$ and $r(t) \geq 0$. Further manipulation of (50), and using (43) yields

$$\dot{V} \leq -w^2\|s\|(1 - \gamma_1\gamma_0)\eta - \frac{b}{a}w^2(1 - \gamma_1\gamma_0)\left(\frac{1}{2}\zeta - r\right)^2 + \frac{b}{4a} \frac{(2 + \gamma_1)^2}{w^2(1 - \gamma_1\gamma_0)} \quad (51)$$

since expanding the quadratic term on the right-hand side of (51) gives the right-hand side of (50). If $\|s\| > \epsilon$, then $w^2\|s\|(1 - \gamma_1\gamma_0)\eta \geq w^2(1 - \gamma_1\gamma_0)\eta\epsilon$. The quantities ϵ, η, a and b are design parameters and so if they are chosen to satisfy

$$\epsilon\eta \geq \frac{b}{4a} \frac{(2 + \gamma_1)^2}{w^4(1 - \gamma_1\gamma_0)^2} = \frac{b}{4a}\zeta^2 \quad (52)$$

then from (51)

$$\dot{V} \leq -\frac{b}{a}w^2(1 - \gamma_1\gamma_0)\left(\frac{1}{2}\zeta - r\right)^2 \leq 0$$

If $\|s\| < \epsilon$ then $D_\epsilon(\|s\|) = 0$ and so substituting in (49) and simplifying terms yields

$$\dot{V} \leq -w^2\|s\|(1 - \gamma_1\gamma_0)\eta - w^2\|s\|(1 - \gamma_1\gamma_0)(l_1\|x(t)\| + l_2)(r(t) - \zeta) - \frac{b}{a}w^2(1 - \gamma_1\gamma_0)(r(t) - \zeta)r(t) \quad (53)$$

Notice by construction $\gamma_1\gamma_0 < 1$ and $r(t) \geq 0$ and therefore for $\|s\| < \epsilon$ and $r(t) > \zeta$, it follows $\dot{V} < 0$. Define a rectangle in \mathbb{R}^2 as

$$\mathcal{R} = \{(\|s\|, r) \mid \|s\| \leq \epsilon, 0 \leq r \leq \zeta\} \quad (54)$$

Also define $\mathcal{R}_+ \in \mathbb{R}^2$ as $\mathcal{R}_+ = \{(\|s\|, r) \mid r \geq 0\}$. By construction of the adaptive gains, $r(t) \geq 0$ for all time and so the trajectory of $(\|s(t)\|, r(t)) \in \mathcal{R}_+$ for all time, and so outside the set $\mathcal{R} \cap \mathcal{R}_+ = \mathcal{R}$, from (51) and (53), the derivative of the Lyapunov function $\dot{V} < 0$. Let \mathcal{V}_d denote the truncated ellipsoid

$$\mathcal{V}_d = \{(\|s\|, r) \mid V(\|s\|, r) \leq d\} \cap \mathcal{R}_+$$

where $V(\cdot)$ is defined in (44). Because \mathcal{R} in (54) is a compact set, for a given $w > 0$, there exists a unique $d_0 > 0$ such that $d_0 = \min\{d \in \mathbb{R}_+ \mid \mathcal{R} \subset \mathcal{V}_d\}$. As shown in Figure 19, since $\mathcal{R} \subset \mathcal{V}_{d_0}$, it follows outside \mathcal{V}_{d_0} the derivative of the Lyapunov function $\dot{V} < 0$ and so \mathcal{V}_{d_0} is an invariant set which is entered in finite time t_0 . Since \mathcal{V}_{d_0} is entered in finite time, $V(\|s\|, r) \leq d_0$ for all $t > t_0$ which implies $\|s\| \leq \sqrt{2d_0/w}$ for $t > t_0$, and hence s enters and remains in a boundary layer of size $\sqrt{2d_0/w}$ around the ideal sliding surface \mathcal{S} . ■

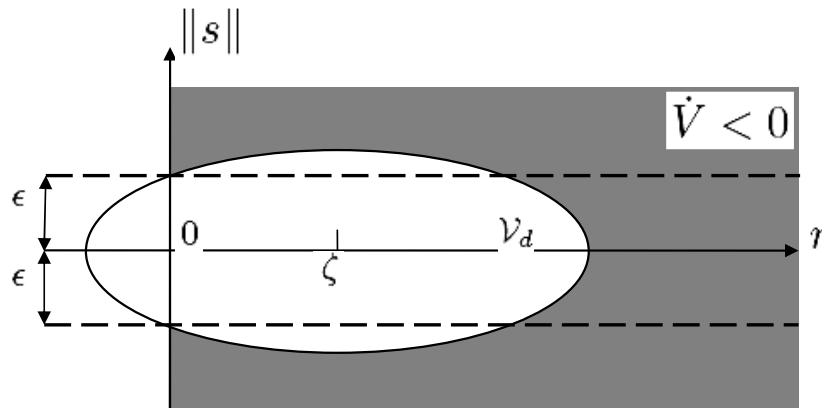


Fig. 19. Level set of the Lyapunov functions V